POLITECNICO DI TORINO

MASTER's Degree in COMMUNICATION ENGINEERING

MASTER's Degree Thesis

Analytical Modeling of Non-Linear Propagation in Long-Haul Optical Transmission Systems

Supervisors

Prof. Pierluigi POGGIOLINI

Dr. Yanchao JIANG

Candidate

Tianchun ZHU

October 2025

Abstract

This thesis presents the complete derivation of **closed-form analytical solutions** for the **Self-Channel Interference (SCI)**, **Cross-Channel Interference (XCI)**, and **Multi-Channel Interference (MCI)** kernel integrals. These integrals are fundamental to the **Polynomial Closed-Form Model (PCFM)** framework, a powerful and innovative approach for modeling nonlinear effects in optical fiber transmission. The predictive accuracy of the PCFM depends directly on the precise evaluation of these integrals. To accomplish this, we used the symbolic computation tool Mathematica, which was essential for handling the complexity of the problem.

The derivation process involved a series of initial mathematical transformations designed to simplify the original complex expressions. This methodical approach allowed us to systematically break down the problem into manageable steps. A crucial and innovative aspect of our methodology was the development of a generalized integral form with symbolic limits. This universal approach allowed us to fully solve the most complex case—the **Multi-Channel Interference (MCI)** integral—and subsequently obtain the analytical solutions for the simpler **SCI** and **XCI** integrals through parameter reduction and elegant substitution. This demonstrates the underlying structure and interconnectedness of these nonlinear effects.

Our work makes a significant contribution to the field of optical transmission by providing an efficient and precise method for calculating **nonlinear interference (NLI)** contributions. These novel analytical solutions pave the way for faster, more accurate modeling of ultra-wideband long-haul system performance, which is essential for the design and optimization of next-generation communication networks. By replacing computationally intensive numerical integrations with these elegant **closed-form expressions**, our work can dramatically accelerate system design and enable real-time performance monitoring, leading to more robust and efficient optical networks.

Contents

1 Introduction

Physical-layer-aware control and optimization of ultra-high-capacity optical networks is becoming an increasingly important aspect of networking, as throughput demand and loads increase. A necessary pre-requisite to achieve it, is the availability of accurate analytical modeling of fiber non-linear effects (or NLI, Non-Linear-Interference). Several NLI models have been proposed over the years, such as 'time-domain' [1,2], GN [3] and EGN [2,4,5], however, these NLI models either contain integrals that make them unsuitable for real-time use, or otherwise assume too idealized system set-ups. Therefore, it becomes significant to derive approximate closed-form formulas (or closed-form model, CFM) which enable real-time computation, while guaranteeing both accuracy preservation and sufficient generality to model highly diverse deployed systems.

In recent years, a series of increasingly accurate closed-form models (CFMs) have been developed, with major contributions from two groups: University College London (UCL) [6, 7] and Politecnico di Torino (PoliTo) in collaboration with CISCO [8,9]. In what follows, we focus on the developments from the PoliTo–OptCom group. The initial formulation, referred to as CFM0, was a closed-form approximation of the incoherent GN model, capable of modeling general WDM systems with varying spans and amplifiers, but limited in its support for some important features such as dispersion slope and loss. This led to the development of CFM1, which incorporated these missing physical parameters to improve modeling realism. However, CFM1 still exhibited an average tendency towards underestimating the SNR due to its GN-based origin and a substantial variance of the error is observed. To address this, CFM2 introduced machine-learned correction laws to achieve significant improvements in both bias and error variance. Yet, outliers with high NLI coherence revealed the limits of the incoherent accumulation assumption, prompting the introduction of CFM3, which explicitly accounted for NLI coherence. Finally, CFM4 added roll-off effects to further enhance modeling accuracy. Together, this progression from CFM0 to CFM4 represents a comprehensive evolution toward a practical and accurate analytical EGN-like model suitable for large-scale, real-time system evaluation [10].

Building upon this modeling framework, a recent experimental study validated the closed-form EGN-like model over a real-world field trial system covering both C and L bands. This work provided the first experimental confirmation of the model's practical accuracy, showing excellent agreement between predicted and measured SNR. The success of this validation underscores the feasibility of applying closed-form analytical EGN-like model on a very wide optical spectrum [11].

Nowadays systems using C+L bands are being widely deployed. Research is exploring

adding further bands, such as S and E, which has highlighted new challenges in multiband environments especially in the presence of strong inter-channel stimulated Raman scattering (ISRS) and backward-pumped Raman amplification. To address these challenges, the CFM5 model was introduced, which accounts for fiber attenuation and power transfer due to ISRS [8, 11]. This was then extended to CFM6, which further incorporates Raman amplification [9]. However, the intricate structure of CFM6, which relies on splitting each span into two sub-spans, presents several limitations: it can lead to inaccuracies in short spans due to loss of intra-span coherence and is hard to upgrade for scenarios like subcarrier multiplexing, ultra-low dispersion, and short spans. To solve these remaining limitations a new modeling approach called the Polynomial Closed-Form Model (PCFM) [12] has been proposed. PCFM expresses the spatial power profile of each channel as a polynomial, enabling near-exact analytical integration of the GN model core terms. PCFM can model multiband systems with ISRS, forward and backward Raman amplification, short spans, lumped loss and other spatial power-profile perturbations. Compared with previous CFMs, it enjoys better accuracy and reliability because it does not rely on either neglecting intra-span NLI coherence or resorting to infinite series expansions, or other problematic approximations. This framework significantly improves modeling fidelity for modern multiband systems and opens the door to even more accurate real-time optimization across extended optical spectra.

Within the framework of Polynomial Closed-Form Models (P-CFMs), integral expressions for self-channel interference (SCI), cross-channel interference (XCI), and multi-channel interference (MCI), based on the polynomial spatial power profile, could be derived [13]. The aim of this paper is to derive analytical solutions to these complex integrals. To facilitate this process, the symbolic computation tool Mathematica is employed. Furthermore, the resulting closed-form expressions are implemented in software and compiled to enable fast numerical evaluation of the desired results.

2 Premises

According to the assumptions and derivations of the incoherent GN model [14], Eq. (1) provides the NLI PSD produced by the generic n_s-th span, $G_{NLI}^{(n_s)}(f)$.

$$G_{\text{NLI}}^{(n_s)}(f) = \frac{16}{27}\Gamma^{(n_s)}(f)\int_{-\infty}^{\infty}\int_{-\infty}^{\infty} G_{\text{WDM}}^{(n_s)}(f_1)G_{\text{WDM}}^{(n_s)}(f_2)G_{\text{WDM}}^{(n_s)}(f_1+f_2-f) \cdot \left(\gamma^{(n_s)}(f_1,f_2,f)\right)^2 \cdot \left|\rho^{(n_s)}(f_1,f_2,f)\right|^2 df_1 df_2,$$

where $\left|\rho^{(n_s)}(f_1,f_2,f)\right|^2 = \left|e^{-\int_0^{L_s^{(n_s)}} \alpha_T^{(n_s)}(f,z)dz}\int_0^{L_s^{(n_s)}} e^{\int_0^z \Delta\kappa^{(n_s)}(f_1,f_2,f,z')dz'}dz\right|^2,$

$$\text{and } \Delta\kappa^{(n_s)}(f_1, f_2, f, z') = -j\left[\beta^{(n_s)}(f_1) + \beta^{(n_s)}(f_2) - \beta^{(n_s)}(f) - \beta^{(n_s)}(f_1 + f_2 - f)\right] - \left[\alpha_T^{(n_s)}(f_1, z') + \alpha_T^{(n_s)}(f_2, z') - \alpha_T^{(n_s)}(f, z') - \alpha_T^{(n_s)}(f_1 + f_2 - f, z')\right]. \quad (1)$$

The variables are defined as follows:

$\Gamma^{(n_s)}(f)$	The frequency-dependent power gain/loss for the n_s-th span.
$G_{\text{WDM}}^{(n_s)}(f)$	The PSD of the WDM signal at the input of the n_s-th span.
f_1, f_2	Dummy variables of integration, representing the frequencies of the interacting channels.
f	The specific frequency where the nonlinear noise PSD is calculated.
$\gamma^{(n_s)}$	The n_s-th span fiber non-linearity coefficient, typically expressed as $1/(\text{W} \cdot \text{km})$.
$L_s^{(n_s)}$	The physical length of the n_s-th fiber span, measured in km.
z	The distance variable along the fiber span, used for integration.
$\alpha_T^{(n_s)}(f, z)$	The total effective attenuation coefficient for the n_s-th span, at frequency f and location z, in the span, in units $1/\text{km}$.
$\beta^{(n_s)}(f)$	The propagation constant (sometimes called "wavenumber") for the n_s-th span, at frequency f and location z in the span, in units ps^2/km.

We can notice that the WDM signal $G_{WDM}^{(n_s)}(f)$ at the input of the n_s-th span appears three times in the integrand function of Eq. (1). To better explain it an example of a possible $G_{WDM}^{(n_s)}(f)$ is shown in Figure 1. Note that the superscript n_s is present because we assume that in each span there can be a different set of WDM channels, that is, a different $G_{WDM}^{(n_s)}(f)$. We also assume that the channel under test (CUT) is present in each span, at the same frequency. All other channels can change, in number, frequency and bandwidth. Specifically, the number of WDM channels in the n_s-th span is $N_{ch}^{(n_s)}$. The set of center frequencies and the set of channel bandwidths in the n_s-th span are:

$$\left\{f_{n_{ch}}^{(n_s)}\right\}_{n_{ch}=1}^{N_{ch}^{(n_s)}}, \quad \left\{B_{n_{ch}}^{(n_s)}\right\}_{n_{ch}=1}^{N_{ch}^{(n_s)}}$$

For any specific span n_s, the CUT is technically one of the channels in that span, with an index $n_{\text{CUT}}^{(n_s)}$ and properties like frequency $f_{n_{\text{CUT}}}^{(n_s)}$ and bandwidth $B_{n_{\text{CUT}}}^{(n_s)}$. However, a key assumption is that the CUT itself never changes from one span to the next. To make the notation cleaner, we'll just use f_{CUT} and B_{CUT} to represent its constant frequency and bandwidth.

We then approximate the channel spectra as rectangles, whose bandwidth is $B_{n_{ch}}^{(n_s)}$. As a

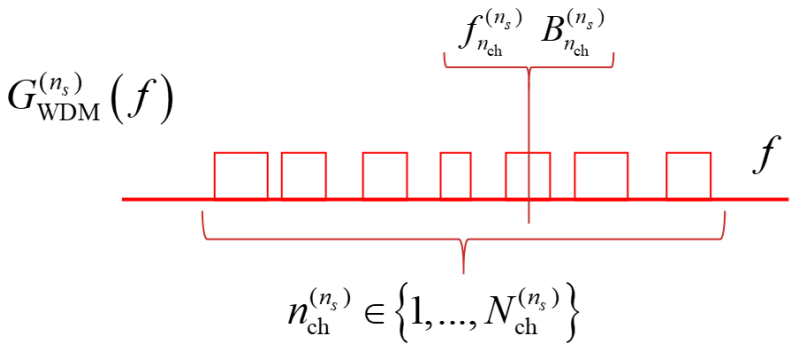

Figure 1: An example of a WDM spectrum $G_{WDM}^{(n_s)}(f)$.

result, we can write the WDM comb at the input of the n_s-th span as:

$$G_{\text{WDM}}^{(n_s)}(f) = \sum_{n_{ch}=1}^{N_{ch}^{(n_s)}} G_{\text{WDM},n_{ch}}^{(n_s)} \cdot \Pi_{B_{n_{ch}}^{(n_s)}}\left(f - f_{n_{ch}}^{(n_s)}\right) \tag{2}$$

where $\Pi_B(f)$ is a Heaviside 'pi' function (i.e., a rectangle) of bandwidth B, defined as:

$$\Pi_B(f) = \begin{cases} 1, & f \in \left[-\frac{B}{2}, \frac{B}{2}\right] \\ 0, & \text{otherwise} \end{cases} \tag{3}$$

and $G_{\text{WDM},n_{ch}}^{(n_s)}$ is the value of the channel PSD, setting the height of the rectangular spectrum.

Regarding the approximation of a channel spectrum with a rectangle in the context of the GN-model, this topic has been discussed in depth in the past, and possibly for the first time in [15]. As time goes by, this approximation seems to become increasingly immaterial, as modern transceivers operate at very small roll-offs, typically on the order of 0.1 or less. Throughout this paper we assume rectangular spectra.

Introducing Eq. (2) into Eq. (1) we get:

$$\begin{aligned} G_{\text{NLI}}^{(n_s)}(f) = \frac{16}{27}\Gamma^{(n_s)}(f) \sum_{k_{ch}=1}^{N_{ch}^{(n_s)}} G_{\text{WDM},k_{ch}}^{(n_s)} \sum_{m_{ch}=1}^{N_{ch}^{(n_s)}} G_{\text{WDM},m_{ch}}^{(n_s)} \sum_{n_{ch}=1}^{N_{ch}^{(n_s)}} G_{\text{WDM},n_{ch}}^{(n_s)} \\ \int_{-\infty}^{\infty}\int_{-\infty}^{\infty} \Pi_{B_{k_{ch}}^{(n_s)}}(f_1 - f_{k_{ch}}^{(n_s)}) \Pi_{B_{m_{ch}}^{(n_s)}}(f_2 - f_{m_{ch}}^{(n_s)}) \Pi_{B_{n_{ch}}^{(n_s)}}(f_1 + f_2 - f - f_{n_{ch}}^{(n_s)}) \\ \cdot \left|\gamma^{(n_s)}(f_1, f_2, f)\right|^2 |\rho(f_1, f_2, f)|^2 \, df_1 df_2 \end{aligned} \tag{4}$$

We then concentrate on calculating $G_{\text{NLI}}^{(n_s)}(f)$ related to a single channel, specifically the CUT. Note that the CUT can be any of the WDM comb channels, so there is actually no

loss of generality in this assumption.

We also limit our interest to finding the PSD of NLI at the center frequency of the CUT, that is $G_{\text{NLI}}^{(n_s)}(f_{\text{CUT}})$. It has been consistently found (for the first time in [15]) that, while not perfectly flat, $G_{\text{NLI}}^{(n_s)}(f)$ is remarkably flat over the bandwidth occupied by each channel. As a result, the assumption of "locally white" NLI noise over each channel, with a PSD value equal to the value that it assumes at the center frequency of the channel, is an accepted and rather accurate approximation. So we can focus our attention on calculating the NLI PSD only at the center of the CUT, that is $G_{\text{NLI}}^{(n_s)}(f_{\text{CUT}})$.

Then:

$$\begin{aligned} G_{\text{NLI}}^{(n_s)}(f_{\text{CUT}}) = \frac{16}{27}\Gamma^{(n_s)}(f) \sum_{k_{ch}=1}^{N_{ch}^{(n_s)}} G_{\text{WDM},k_{ch}}^{(n_s)} \sum_{m_{ch}=1}^{N_{ch}^{(n_s)}} G_{\text{WDM},m_{ch}}^{(n_s)} \sum_{n_{ch}=1}^{N_{ch}^{(n_s)}} G_{\text{WDM},n_{ch}}^{(n_s)} \\ \int_{-\infty}^{\infty}\int_{-\infty}^{\infty} \Pi_{B_{k_{ch}}^{(n_s)}}(f_1 - f_{k_{ch}}^{(n_s)}) \Pi_{B_{m_{ch}}^{(n_s)}}(f_2 - f_{m_{ch}}^{(n_s)}) \Pi_{B_{n_{ch}}^{(n_s)}}(f_1 + f_2 - f - f_{n_{ch}}^{(n_s)}) \\ \cdot \left|\gamma^{(n_s)}(f_1, f_2, f)\right|^2 |\rho(f_1, f_2, f)|^2 \, df_1 df_2 \end{aligned} \tag{5}$$

Each of the terms of the triple summation then creates a specific integration domain in f_1 and f_2. Specifically, considering a generic term of the triple summation, the integration domain for f_1 and f_2 results from the intersection of three conditions:

$$\begin{aligned} f_1 &\in \left[f_{k_{ch}}^{(n_s)} - B_{k_{ch}}^{(n_s)}/2, f_{k_{ch}}^{(n_s)} + B_{k_{ch}}^{(n_s)}/2\right] \\ &\text{due to} \quad \Pi_{B_{k_{ch}}^{(n_s)}}\left(f_1 - f_{k_{ch}}^{(n_s)}\right) \\ f_2 &\in \left[f_{m_{ch}}^{(n_s)} - B_{m_{ch}}^{(n_s)}/2, f_{m_{ch}}^{(n_s)} + B_{m_{ch}}^{(n_s)}/2\right] \\ &\text{due to} \quad \Pi_{B_{m_{ch}}^{(n_s)}}\left(f_2 - f_{m_{ch}}^{(n_s)}\right) \\ f_1 + f_2 &\in \left[f_{\text{CUT}} + f_{n_{ch}}^{(n_s)} - B_{n_{ch}}^{(n_s)}/2, f_{\text{CUT}} + f_{n_{ch}}^{(n_s)} + B_{n_{ch}}^{(n_s)}/2\right] \\ &\text{due to} \quad \Pi_{B_{n_{ch}}^{(n_s)}}\left(f_1 + f_2 - f_{\text{CUT}} - f_{n_{ch}}^{(n_s)}\right) \end{aligned}$$

The resulting integration domain is made up of distinct sub-domains, sometimes called "islands". Reference [13] provides an example of a 7-channel WDM comb with equally spaced, identical-bandwidth channels, where the CUT is the center channel. The corresponding integration plane is shown in Figure 2.

The islands along the two axes going through the center frequency of the CUT, which are marked in yellow and red, contribute the most to NLI. The yellow ones represent the Cross-Channel Interference (XCI) islands and the red one at the center represents Self-

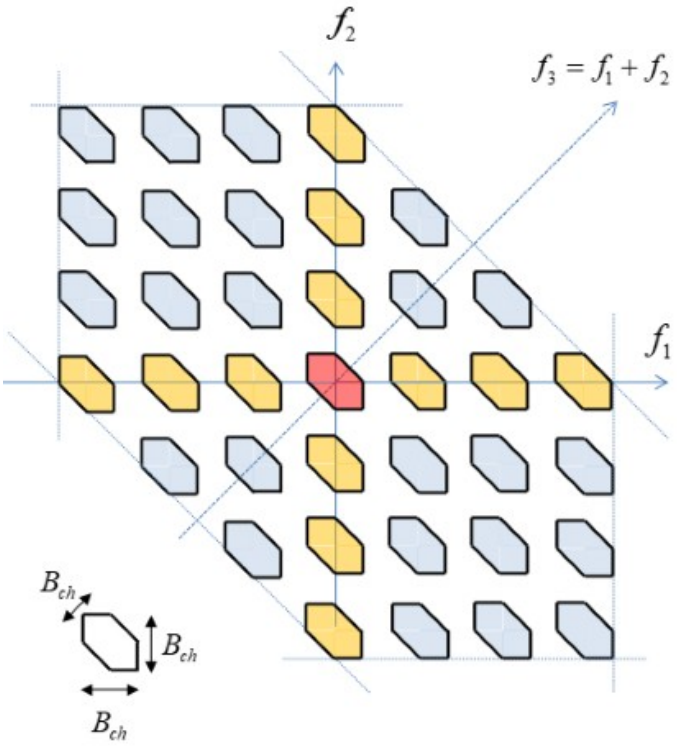

Figure 2: Integration domain "islands".

Channel Interference (SCI) island. As for the gray islands, they are Multi-Channel Interference (MCI) islands, of which the contribution to NLI is negligible in a high-dispersion context. We can find in Figure 2 that the yellow XCI islands and the red SCI island share a common center frequency on one axis while differing on the orthogonal axis, whereas the MCI islands do not share a common center frequency with the SCI island on either the f_1 or f_2 axis.

In [16] the expression for the NLI PSD contribution of any generic island x (approximated as a rectangle) in any generic span n_s is derived and it is:

$$G_{\mathrm{NLL},x}^{(n_s)}(f_{\mathrm{CUT}}) = \frac{16}{27}\Gamma^{(n_s)}(f_{\mathrm{CUT}}) \cdot G_{\mathrm{WDM},k_{\mathrm{ch}}}^{(n_s)} G_{\mathrm{WDM},m_{\mathrm{ch}}}^{(n_s)} G_{\mathrm{WDM},n_{\mathrm{ch}}}^{(n_s)} (\gamma_x^{(n_s)})^2 p_{\mathrm{CUT}}^{(n_s)} (L_s^{(n_s)}) \cdot \int_{f_{m_{\mathrm{ch}}}^{(n_s)} - f_{\mathrm{CUT}} - B_{m_{\mathrm{ch}}}^{(n_s)}/2}^{f_{m_{\mathrm{ch}}}^{(n_s)} - f_{\mathrm{CUT}} + B_{m_{\mathrm{ch}}}^{(n_s)}/2} \int_{f_{k_{\mathrm{ch}}}^{(n_s)} - f_{\mathrm{CUT}} - B_{k_{\mathrm{ch}}}^{(n_s)}/2}^{f_{k_{\mathrm{ch}}}^{(n_s)} - f_{\mathrm{CUT}} + B_{k_{\mathrm{ch}}}^{(n_s)}/2} \left| \int_0^{L_s^{(n_s)}} p_x^{(n_s)}(z) e^{j4\pi^2 f_1' f_2' \beta_{2,\mathrm{eff},x}^{(n_s)} z} dz \right|^2 df_1' df_2' \tag{6}$$

where:

$$\begin{aligned} f_1 &= f_1' + f_{\mathrm{CUT}} \\ f_2 &= f_2' + f_{\mathrm{CUT}} \end{aligned} \tag{7}$$

This is tantamount to centering the new axes f_1' and f_2' at the point $(0,0)$ in the new coordinates. Essentially, this simply means that the axes are centered on the CUT. As each channel becomes the CUT, the axes are moved onto its frequency. To better describe it an example is given through Figure 3.

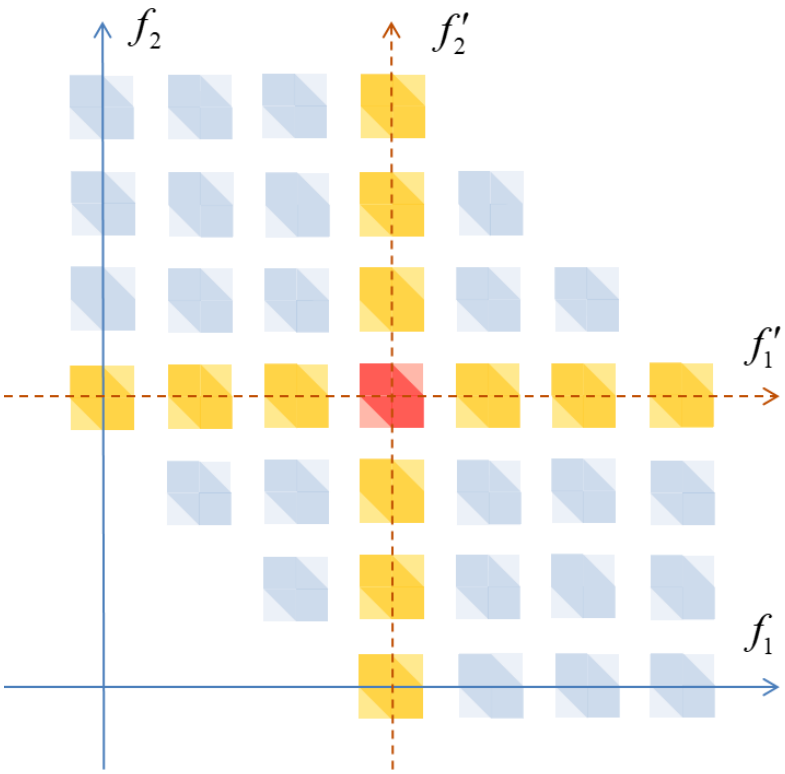

Figure 3: Integration domain 'islands' for a 7-channel WDM comb of equally spaced and identical-bandwidth channels. The origin of the frequency axes (f_1, f_2) is set to the frequency of the lowest-frequency WDM channel, whereas the origin of the (f_1', f_2') axes is set to the center frequency of the CUT. The lighter colored shading means the lozenge-shaped integration domains are approximated as squares.

The important formula (6) shows that the key analytical hurdle to achieving a CFM is solving for the integral 'kernel', which we call $K_x^{(n_s)}(f_{\text{CUT}})$:

$$K_x^{(n_s)}(f_{\text{CUT}}) = \int_{f_{m_{\text{ch}}}^{(n_s)} - f_{\text{CUT}} - B_{m_{\text{ch}}}^{(n_s)}/2}^{f_{m_{\text{ch}}}^{(n_s)} - f_{\text{CUT}} + B_{m_{\text{ch}}}^{(n_s)}/2} \int_{f_{k_{\text{ch}}}^{(n_s)} - f_{\text{CUT}} - B_{k_{\text{ch}}}^{(n_s)}/2}^{f_{k_{\text{ch}}}^{(n_s)} - f_{\text{CUT}} + B_{k_{\text{ch}}}^{(n_s)}/2} \cdot \left| \int_0^{L_s^{(n_s)}} p_x^{(n_s)}(z) e^{j4\pi^2 f_1' f_2' \beta_{2,\text{eff},x}^{(n_s)} z} dz \right|^2 df_1' df_2' \quad (8)$$

Then we can focus on analytically dealing with these integral kernels. First let us focus on the yellow XCI islands straddling the horizontal f_1' axis, i.e., the axis with $f_2' = 0$ (see

Figure 4). We call them 'horizontal axis' XCI islands.

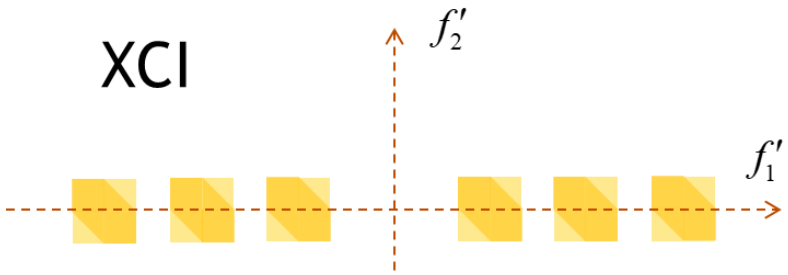

Figure 4: XCI islands on the horizontal axis.

By imposing $m_{\text{ch}}^{(n_s)} = n_{\text{CUT}}^{(n_s)}$ and $k_{\text{ch}}^{(n_s)} = n_{\text{ch}}^{(n_s)}$, with $n_{\text{ch}} = 1 \dots N_{\text{ch}}$ and $n_{\text{ch}} \neq n_{\text{CUT}}$ because $n_{\text{ch}} = n_{\text{CUT}}$ would be SCI, we can get:

$$K_{\text{XCI,h}}^{(n_s)} = \int_{-B_{\text{CUT}}/2}^{B_{\text{CUT}}/2} \int_{f_{n_{\text{ch}}}^{(n_s)} - f_{\text{CUT}} - B_{n_{\text{ch}}}^{(n_s)}/2}^{f_{n_{\text{ch}}}^{(n_s)} - f_{\text{CUT}} + B_{n_{\text{ch}}}^{(n_s)}/2} \left| \int_0^{L_s^{(n_s)}} e^{j4\pi^2 f_1' f_2' \cdot \beta_{2,\text{eff},n_{\text{ch}}}^{(n_s)} \cdot z} \cdot p_{n_{\text{ch}}}^{(n_s)}(z)\, dz \right|^2 df_1' df_2' \quad (9)$$

We then focus on the yellow XCI islands straddling the vertical f_2' axis, i.e., the axis with $f_1' = 0$. We call them 'vertical axis' XCI islands. By imposing $k_{\text{ch}}^{(n_s)} = n_{\text{CUT}}^{(n_s)}$ and $m_{\text{ch}}^{(n_s)} = n_{\text{ch}}^{(n_s)}$, again with $n_{\text{ch}} = 1 \dots N_{\text{ch}}$ and $n_{\text{ch}} \neq n_{\text{CUT}}$, we can get:

$$K_{\text{XCI,v}}^{(n_s)} = \int_{-B_{\text{CUT}}/2}^{B_{\text{CUT}}/2} \int_{f_{n_{\text{ch}}}^{(n_s)} - f_{\text{CUT}} - B_{n_{\text{ch}}}^{(n_s)}/2}^{f_{n_{\text{ch}}}^{(n_s)} - f_{\text{CUT}} + B_{n_{\text{ch}}}^{(n_s)}/2} \left| \int_0^{L_s^{(n_s)}} e^{j4\pi^2 f_1' f_2' \cdot \beta_{2,\text{eff},n_{\text{ch}}}^{(n_s)} \cdot z} \cdot p_{n_{\text{ch}}}^{(n_s)}(z)\, dz \right|^2 df_2' df_1' \quad (10)$$

The core distinction between Eq. (9) and Eq. (10) lies solely in the reversed sequence of the differential variables, df_1' and df_2'. This difference is immaterial, however, because a straightforward change of integration variables—specifically, exchanging f_1' and f_2'—demonstrates that the results of the two equations are identical for any given $n_{\text{CUT}}^{(n_s)}$ and $n_{\text{ch}}^{(n_s)}$. Consequently, to account for the total XCI contribution, we can calculate the integral for only the horizontal axis XCI islands and double that result. Therefore, we will henceforth treat the horizontal axis XCI islands as the representative case for all XCI calculations, that is:

$$K_{\text{XCI},n_{\text{ch}}}^{(n_s)} = \int_{-B_{\text{CUT}}/2}^{B_{\text{CUT}}/2} \int_{f_{n_{\text{ch}}}^{(n_s)} - f_{\text{CUT}} - B_{n_{\text{ch}}}^{(n_s)}/2}^{f_{n_{\text{ch}}}^{(n_s)} - f_{\text{CUT}} + B_{n_{\text{ch}}}^{(n_s)}/2} \left| \int_0^{L_s^{(n_s)}} e^{j4\pi^2 f_1' f_2' \cdot \beta_{2,\text{eff},n_{\text{ch}}}^{(n_s)} \cdot z} \cdot p_{n_{\text{ch}}}^{(n_s)}(z)\, dz \right|^2 df_1' df_2' \tag{11}$$

We can then obtain the expression for the NLI PSD contribution of XCI island as:

$$G_{\text{NLI,XCI}}^{(n_s)}(f_{\text{CUT}}) = \frac{16}{27} \cdot p_{\text{CUT}}^{(n_s)}(L_s^{(n_s)}) \cdot \Gamma^{(n_s)}(f_{\text{CUT}}) \cdot G_{\text{CUT}}^{(n_s)} \cdot (G_{\text{WDM},n_{\text{ch}}}^{(n_s)})^2 \cdot (\gamma_{\text{XCI}}^{(n_s)})^2 \cdot K_{\text{XCI},n_{\text{ch}}}^{(n_s)} \tag{12}$$

Then let us focus on the SCI integration that takes place over the red islands represented in the examples of Figure 2. In the SCI island, we have:

$$f_{k_{\text{ch}}}^{(n_s)} = f_{m_{\text{ch}}}^{(n_s)} = f_{n_{\text{ch}}}^{(n_s)} = f_{\text{CUT}}$$

$$B_{k_{\text{ch}}}^{(n_s)} = B_{m_{\text{ch}}}^{(n_s)} = B_{n_{\text{ch}}}^{(n_s)} = B_{\text{CUT}}$$

Therefore we get for SCI:

$$K_{\text{SCL,CUT}}^{(n_s)} = \int_{-B_{\text{CUT}}/2}^{B_{\text{CUT}}/2} \int_{-B_{\text{CUT}}/2}^{B_{\text{CUT}}/2} \left| \int_0^{L_s^{(n_s)}} e^{j4\pi^2 f_1' f_2' \cdot \beta_{2,\text{eff,CUT}}^{(n_s)} \cdot z} \cdot p_{\text{CUT}}^{(n_s)}(z)\, dz \right|^2 df_1' df_2' \tag{13}$$

Also we can obtain the expression for the NLI PSD contribution of SCI island as:

$$G_{\text{SCI}}^{(n_s)}(f_{\text{CUT}}) = \frac{16}{27} \cdot p_{\text{CUT}}^{(n_s)}(L_s^{(n_s)}) \cdot \Gamma^{(n_s)}(f_{\text{CUT}}) \cdot (G_{\text{CUT}}^{(n_s)})^3 \cdot |\gamma_{\text{SCI}}^{(n_s)}|^2 \cdot K_{\text{SCL,CUT}}^{(n_s)} \tag{14}$$

Regarding MCI islands, visually represented in gray (see Figure 2), current research often overlooks their contribution, primarily due to the prevailing assumption of systems operating with high dispersion and large symbol rates. Given the objectives of this paper, it is necessary to analyze this contribution. Following its definition, we can formally define the MCI island identifiers using the original indices k_{ch} and m_{ch}, where k_{ch} and m_{ch} traverse the channel indices $1 \ldots N_{\text{ch}}$, with the crucial constraint that both k_{ch} and m_{ch} must be unequal to n_{CUT}. The integral expression for the MCI kernel is thus implied by these definitions, leading to:

$$K^{(n_s)}_{\text{MCI},k_{\text{ch}},m_{\text{ch}}} = \int_{f^{(n_s)}_{m_{\text{ch}}}-f_{\text{CUT}}-B^{(n_s)}_{m_{\text{ch}}}/2}^{f^{(n_s)}_{m_{\text{ch}}}-f_{\text{CUT}}+B^{(n_s)}_{m_{\text{ch}}}/2} \int_{f^{(n_s)}_{k_{\text{ch}}}-f_{\text{CUT}}-B^{(n_s)}_{k_{\text{ch}}}/2}^{f^{(n_s)}_{k_{\text{ch}}}-f_{\text{CUT}}+B^{(n_s)}_{k_{\text{ch}}}/2} \cdot \left| \int_0^{L^{(n_s)}_s} e^{j4\pi^2 f'_1 f'_2 \cdot \beta^{(n_s)}_{2,\text{eff},k_{\text{ch}},m_{\text{ch}}} \cdot z} \cdot p^{(n_s)}_{k_{\text{ch}},m_{\text{ch}}}(z)\, dz \right|^2 df'_1 df'_2 \tag{15}$$

Then expression for the NLI PSD contribution of MCI island is:

$$G^{(n_s)}_{\text{MCI}}(f_{\text{CUT}}) = \frac{16}{27} \cdot p^{(n_s)}_{\text{CUT}}(L^{(n_s)}_s) \cdot \Gamma^{(n_s)}(f_{\text{CUT}}) \cdot G^{(n_s)}_{\text{WDM},n_{\text{ch}}} \cdot G^{(n_s)}_{\text{WDM},k_{\text{ch}}} \cdot G^{(n_s)}_{\text{WDM},m_{\text{ch}}} \cdot |\gamma^{(n_s)}_{\text{MCI}}|^2 \cdot K^{(n_s)}_{\text{MCI},k_{\text{ch}},m_{\text{ch}}} \tag{16}$$

We assume that the channel spatial power-profile has a polynomial form:

$$p(z) \approx p_0 + p_1 \cdot z + p_2 \cdot z^2 + \cdots + p_n \cdot z^n + \cdots + p_{N_p} \cdot z^{N_p} = \sum_{n=0}^{N_p} p_n \cdot z^n \tag{17}$$

Then with substitution we could get:

$$K^{(n_s)}_{\text{XCI},n_{ch}} = \int_{-B_{\text{CUT}}/2}^{B_{\text{CUT}}/2} \int_{f^{(n_s)}_{n_{\text{ch}}}-f_{\text{CUT}}-B^{(n_s)}_{n_{ch}}/2}^{f^{(n_s)}_{n_{\text{ch}}}-f_{\text{CUT}}+B^{(n_s)}_{n_{ch}}/2} \left| \int_0^{L^{(n_s)}_s} e^{j4\pi^2 f'_1 f'_2 \cdot \beta^{(n_s)}_{2,\text{eff},n_{ch}} \cdot z} \cdot \left[\sum_{n=0}^{N_p} p^{(n_s)}_{n,n_{ch}} \cdot z^n \right] dz \right|^2 df'_1 df'_2 \tag{18}$$

$$K^{(n_s)}_{\text{SCI,CUT}} = \int_{-B_{\text{CUT}}/2}^{B_{\text{CUT}}/2} \int_{-B_{\text{CUT}}/2}^{B_{\text{CUT}}/2} \left| \int_0^{L^{(n_s)}_s} e^{j4\pi^2 f'_1 f'_2 \cdot \beta^{(n_s)}_{2,\text{eff,CUT}} \cdot z} \cdot \left[\sum_{n=0}^{N_p} p^{(n_s)}_{n,\text{CUT}} \cdot z^n \right] dz \right|^2 df'_1 df'_2 \tag{19}$$

$$K^{(n_s)}_{\text{MCI},k_{\text{ch}},m_{\text{ch}}} = \int_{f^{(n_s)}_{m_{\text{ch}}}-f_{\text{CUT}}-B^{(n_s)}_{m_{\text{ch}}}/2}^{f^{(n_s)}_{m_{\text{ch}}}-f_{\text{CUT}}+B^{(n_s)}_{m_{\text{ch}}}/2} \int_{f^{(n_s)}_{k_{\text{ch}}}-f_{\text{CUT}}-B^{(n_s)}_{k_{\text{ch}}}/2}^{f^{(n_s)}_{k_{\text{ch}}}-f_{\text{CUT}}+B^{(n_s)}_{k_{\text{ch}}}/2} \cdot \left| \int_0^{L^{(n_s)}_s} e^{j4\pi^2 f'_1 f'_2 \cdot \beta^{(n_s)}_{2,\text{eff},k_{\text{ch}},m_{\text{ch}}} \cdot z} \cdot \left[\sum_{n=0}^{N_p} p^{(n_s)}_{n,k_{\text{ch}},m_{\text{ch}}} \cdot z^n \right] dz \right|^2 df'_1 df'_2 \tag{20}$$

In systems featuring high dispersion and large symbol rates, a substantial simplification can be achieved for XCI by executing the outer integral in Eq. (18) between $[-\infty, \infty]$ rather than $[-B_{\text{CUT}}/2, B_{\text{CUT}}/2]$. This simplification is possible because the nature of the

integrand is such that $\beta^{(n_s)}_{2,\text{eff},n_{\text{ch}}}$ sets the decay rate of the integrand as it moves away from the axes. Critically, the more dispersion is present, the faster the decay is. Consequently, the added integration region contributes a small, and typically negligible, amount to the total integral. Once the stretching of the integration region has been performed, the XCI kernel integrals admit a fully closed-form exact solution (no further approximation):

$$K^{(n_s)}_{\text{XCI},n_{\text{ch}}} = \frac{L_s^{(n_s)}}{2\pi \left|\beta^{(n_s)}_{2,\text{eff},n_{\text{ch}}}\right|} \cdot \log \left| \frac{f^{(n_s)}_{n_{\text{ch}}} - f_{\text{CUT}} + B^{(n_s)}_{n_{\text{ch}}}/2}{f^{(n_s)}_{n_{\text{ch}}} - f_{\text{CUT}} - B^{(n_s)}_{n_{\text{ch}}}/2} \right| \cdot \sum_{n=0}^{N_p} \sum_{k=0}^{N_p} \frac{p^{(n_s)}_{n,n_{\text{ch}}} p^{(n_s)}_{k,n_{\text{ch}}} \left(L_s^{(n_s)}\right)^{(n+k)}}{n+k+1} \tag{21}$$

As for SCI, it is unlike the XCI case. Here, it is not possible to stretch the integration domain to infinity along either one of the axes. The reason is that integration to infinity straddling either one of the axes inevitably results in divergence. The SCI kernel therefore needs to be integrated without any further approximations.

In this paper, we move beyond the constraints of pre-made assumptions. We focus on deriving all exact analytical solutions for the integral kernels of self-channel interference (SCI), cross-channel interference (XCI), and mixed-channel interference (MCI). These rigorous solutions enable the assessment of the Nonlinear Interference (NLI) Power Spectral Density (PSD) in a fully general and context-independent manner, meaning the simplification described above will not be employed.

3 Integrals to work on

The integral expressions shown above are the main subject of our analysis. However, inputting these complete, multi-level integrals directly into a symbolic computation tool like Mathematica is challenging, as their complexity can lead to excessively long computation times or unevaluated results.

To obtain the analytical solutions efficiently, it is necessary to first perform some mathematical manipulations on the integral expressions. We will now break down the integral structure step-by-step to transform it into a form that is more suitable for symbolic computation.

3.1 The SCI kernel

Let us start with the SCI kernel first, see Eq. (19). To simplify the notation for derivation purposes, we rewrite the SCI integral in a general form:

$$K_{\text{SCI}} = \int_{-B/2}^{B/2} \int_{-B/2}^{B/2} \left| \sum_{n=0}^{N_p} p_n \cdot \int_0^L e^{j4\pi^2 f_1 f_2 \cdot \beta \cdot z} \cdot z^n \, dz \right|^2 df_1 df_2 \tag{22}$$

The innermost integral needs to be absolute-value squared. Given a complex quantity q, its absolute value squared is qq^*. We can write:

$$\begin{aligned} \left| \sum_{n=0}^{N_p} p_n \int_0^L e^{j4\pi^2 f_1 f_2 \cdot \beta \cdot z} \cdot z^n \, dz \right|^2 = & \left(\sum_{n=0}^{N_p} p_n \int_0^L e^{j4\pi^2 f_1 f_2 \cdot \beta \cdot z} \cdot z^n \, dz \right) \\ & \cdot \left(\sum_{n=0}^{N_p} p_n \int_0^L e^{j4\pi^2 f_1 f_2 \cdot \beta \cdot z} \cdot z^n \, dz \right)^* \end{aligned} \tag{23}$$

To further manipulate the formula, we can rename the dummy integration variables to z_1 and z_2 so that they do not get mixed up when we combine the integrals:

$$\begin{aligned} & \left(\sum_{n=0}^{N_p} p_n \int_0^L e^{j4\pi^2 f_1 f_2 \cdot \beta \cdot z} \cdot z^n \, dz \right) \left(\sum_{n=0}^{N_p} p_n \int_0^L e^{j4\pi^2 f_1 f_2 \cdot \beta \cdot z} \cdot z^n \, dz \right)^* \\ & \quad = \left(\sum_{n=0}^{N_p} p_n \int_0^L e^{j4\pi^2 f_1 f_2 \cdot \beta \cdot z_1} \cdot z_1^n \, dz_1 \right) \left(\sum_{m=0}^{N_p} p_m \int_0^L e^{j4\pi^2 f_1 f_2 \cdot \beta \cdot z_2} \cdot z_2^m \, dz_2 \right)^* \end{aligned} \tag{24}$$

Now we can manipulate the two terms and recognize the following derivation:

$$\begin{aligned} & \left| \sum_{n=0}^{N_p} p_n \int_0^L e^{j4\pi^2 f_1 f_2 \cdot \beta \cdot z} \cdot z^n \, dz \right|^2 \\ & = \left(\sum_{n=0}^{N_p} p_n \int_0^L e^{j4\pi^2 f_1 f_2 \cdot \beta \cdot z_1} \cdot z_1^n \, dz_1 \right) \left(\sum_{m=0}^{N_p} p_m \int_0^L e^{j4\pi^2 f_1 f_2 \cdot \beta \cdot z_2} \cdot z_2^m \, dz_2 \right)^* \\ & = \sum_{n=0}^{N_p} \sum_{m=0}^{N_p} p_n p_m^* \int_0^L e^{j4\pi^2 f_1 f_2 \cdot \beta \cdot z_1} \cdot z_1^n \, dz_1 \int_0^L e^{-j4\pi^2 f_1 f_2 \cdot \beta \cdot z_2} \cdot z_2^m \, dz_2 \\ & = \sum_{n=0}^{N_p} \sum_{m=0}^{N_p} p_n p_m^* \int_0^L \int_0^L e^{j4\pi^2 f_1 f_2 \cdot \beta \cdot z_1} e^{-j4\pi^2 f_1 f_2 \cdot \beta \cdot z_2} \cdot z_1^n z_2^m \, dz_1 dz_2 \\ & = \sum_{n=0}^{N_p} \sum_{m=0}^{N_p} p_n p_m^* \int_0^L \int_0^L e^{j4\pi^2 f_1 f_2 \cdot \beta \cdot (z_1 - z_2)} \cdot z_1^n z_2^m \, dz_1 dz_2 \end{aligned} \tag{25}$$

Note that the quantities p_m and z_2 should formally have been complex-conjugated, but since they are real quantities, the conjugation has no effect. Using this result, we can

rewrite the full K_{SCI} integral and move the summations outside the integrals:

$$\begin{aligned} K_{\text{SCI}} &= \int_{-B/2}^{B/2} \int_{-B/2}^{B/2} \left| \int_0^L e^{j4\pi^2 f_1 f_2 \cdot \beta \cdot z} \cdot \sum_{n=0}^{N_p} p_n \cdot z^n \, dz \right|^2 df_1 df_2 \\ &= \int_{-B/2}^{B/2} \int_{-B/2}^{B/2} \sum_{n=0}^{N_p} \sum_{m=0}^{N_p} p_n p_m \cdot \int_0^L \int_0^L e^{j4\pi^2 f_1 f_2 \cdot \beta \cdot (z_1 - z_2)} \cdot z_1^n z_2^m \, dz_1 dz_2 \, df_1 df_2 \\ &= \sum_{n=0}^{N_p} \sum_{m=0}^{N_p} p_n p_m \int_{-B/2}^{B/2} \int_{-B/2}^{B/2} \int_0^L \int_0^L e^{j4\pi^2 f_1 f_2 \cdot \beta \cdot (z_1 - z_2)} \cdot z_1^n z_2^m \, dz_1 dz_2 \, df_1 df_2 \end{aligned}$$

If we define the four-fold integral as Q_{nm}:

$$Q_{nm} = \int_{-B/2}^{B/2} \int_{-B/2}^{B/2} \int_0^L \int_0^L e^{j4\pi^2 f_1 f_2 \cdot \beta \cdot (z_1 - z_2)} \cdot z_1^n z_2^m \, dz_1 dz_2 \, df_1 df_2 \tag{26}$$

Then we can write, very compactly:

$$K_{\text{SCI}} = \sum_{n=0}^{N_p} \sum_{m=0}^{N_p} p_n p_m \cdot Q_{nm} \tag{27}$$

This shows that the fundamental integrals to solve are the Q_{nm}. After solving them, fast code for the actual calculation of the solution based on the closed-form result needs to be written as well.

The first goal is to find the analytical solution for all the:

$$Q_{nm} = \int_{-B/2}^{B/2} \int_{-B/2}^{B/2} \int_0^L \int_0^L e^{j4\pi^2 f_1 f_2 \cdot \beta \cdot (z_1 - z_2)} \cdot z_1^n z_2^m \, dz_1 dz_2 \, df_1 df_2$$

One problem though is that the individual Q_{nm} are complex. This may seem strange since they originate from an absolute value squared. However, while the overall sum in Eq. (27) is real, the individual Q_{nm} are not.

There is though a way to find fundamental integrals similar to the Q_{nm} that are real. This hinges on the remark that in Eq. (27) the two summations go through the same indices (from 1 to N_p) and therefore for each term Q_{nm} that they generate, they also generate a term Q_{mn}. In fact, there are always contributions to the sum in pairs:

$$p_n p_m \cdot Q_{nm} \quad , \quad p_m p_n \cdot Q_{mn}$$

except for when $n = m$ in which case we simply get one contribution $p_n p_n \cdot Q_{nn} = p_n^2 Q_{nn}$.

This allows to re-write the summation as:

$$K_{\text{SCI}} = \sum_{n=0}^{N_p} \sum_{m=n+1}^{N_p} p_n p_m (Q_{nm} + Q_{mn}) + \sum_{n=0}^{N_p} p_n^2 Q_{nn} \tag{28}$$

We can then define:

$$I_{nm} = Q_{nm} + Q_{mn} \tag{29}$$

$$I_{nn} = Q_{nn} \tag{30}$$

and write:

$$K_{\text{SCI}} = \sum_{n=0}^{N_p} \sum_{m=n+1}^{N_p} p_n p_m \cdot I_{nm} + \sum_{n=0}^{N_p} p_n^2 \cdot I_{nn} \tag{31}$$

This formulation is advantageous because it renders all integrals, I_{nm} and I_{nn}, real-valued, thereby eliminating the complex component.

The integrals for the cross-terms ($n \neq m$) are derived from the sum of two symmetric contributions (Q_{nm} and Q_{mn}), resulting in I_{nm}:

$$\begin{aligned} I_{nm} &= Q_{nm} + Q_{mn} \\ &= \int_{-B/2}^{B/2} \int_{-B/2}^{B/2} \int_0^L \int_0^L e^{j4\pi^2 f_1 f_2 \cdot \beta \cdot (z_1 - z_2)} \cdot z_1^n z_2^m \, dz_1 dz_2 \, df_1 df_2 \\ &\quad + \int_{-B/2}^{B/2} \int_{-B/2}^{B/2} \int_0^L \int_0^L e^{j4\pi^2 f_1 f_2 \cdot \beta \cdot (z_2 - z_1)} \cdot z_2^n z_1^m \, dz_2 dz_1 \, df_1 df_2 \\ &= \int_{-B/2}^{B/2} \int_{-B/2}^{B/2} \int_0^L \int_0^L e^{j4\pi^2 f_1 f_2 \cdot \beta \cdot (z_1 - z_2)} \cdot (z_1^n z_2^m + z_1^m z_2^n) \, dz_1 dz_2 \, df_1 df_2 \end{aligned} \tag{32}$$

Or compactly:

$$I_{nm} = \int_{-B/2}^{B/2} \int_{-B/2}^{B/2} \int_0^L \int_0^L e^{j4\pi^2 f_1 f_2 \cdot \beta \cdot (z_1 - z_2)} \cdot (z_1^n z_2^m + z_1^m z_2^n) \, dz_1 dz_2 \, df_1 df_2 \tag{33}$$

Conversely, the integral for the self-terms ($n = m$) requires only one contribution (Q_{nn}) and is defined as I_{nn}:

$$I_{nn} = Q_{nn} = \int_{-B/2}^{B/2} \int_{-B/2}^{B/2} \int_0^L \int_0^L e^{j4\pi^2 f_1 f_2 \cdot \beta \cdot (z_1 - z_2)} \cdot z_1^n z_2^n \, dz_1 dz_2 \, df_1 df_2 \tag{34}$$

With the final result being shown as Eq. (31).

3.2 The XCI and MCI kernels

Using the same decomposition method, we can derive the corresponding real integrals for the XCI and MCI cases. Therefore, we will not repeat the derivation from Section 3.1 and will instead present the corresponding results directly.

3.2.1 XCI Kernel

As what we did above in Section 3.1 to simplify the notation, the general form of the K_{XCI} integral can be written as:

$$K_{\text{XCI}} = \int_{-B_{\text{CUT}}/2}^{B_{\text{CUT}}/2} \int_{f_{\text{ch}}-f_{\text{CUT}}-B_{\text{ch}}}^{f_{\text{ch}}-f_{\text{CUT}}+B_{\text{ch}}} \left| \sum_{n=0}^{N_p} p_n \cdot \int_0^L e^{j4\pi^2 f_1 f_2 \cdot \beta \cdot z} \cdot z^n \, dz \right|^2 df_1 df_2 \tag{35}$$

Following the procedure established in Section 3.1 (SCI), we apply the same decomposition to convert the complex core integral into a sum of real-valued integrals, maintaining the distinction between the $n \neq m$ cross-terms and the $n = m$ self-terms. The corresponding real-valued integrals are:

$$I_{nm,\text{XCI}} = \int_{-B_{\text{CUT}}/2}^{B_{\text{CUT}}/2} \int_{f_{\text{ch}}-f_{\text{CUT}}-B_{\text{ch}}}^{f_{\text{ch}}-f_{\text{CUT}}+B_{\text{ch}}} \int_0^L \int_0^L e^{j4\pi^2 f_1 f_2 \cdot \beta \cdot (z_1 - z_2)} (z_1^n z_2^m + z_1^m z_2^n) \, dz_1 dz_2 \, df_1 df_2 \tag{36}$$

$$I_{nn,\text{XCI}} = \int_{-B_{\text{CUT}}/2}^{B_{\text{CUT}}/2} \int_{f_{\text{ch}}-f_{\text{CUT}}-B_{\text{ch}}}^{f_{\text{ch}}-f_{\text{CUT}}+B_{\text{ch}}} \int_0^L \int_0^L e^{j4\pi^2 f_1 f_2 \cdot \beta \cdot (z_1 - z_2)} z_1^n z_2^n \, dz_1 dz_2 \, df_1 df_2 \tag{37}$$

And the final result is:

$$K_{\text{XCI}} = \sum_{n=0}^{N_p} \sum_{m=n+1}^{N_p} p_n p_m \cdot I_{nm,\text{XCI}} + \sum_{n=0}^{N_p} p_n^2 \cdot I_{nn,\text{XCI}} \tag{38}$$

3.2.2 MCI Kernel

Also we can simplify the notation by writting the general form of the K_{MCI} integral as:

$$K_{\text{MCI}} = \int_{f_{\text{ch},2}-f_{\text{CUT}}-B_{\text{ch},2}}^{f_{\text{ch},2}-f_{\text{CUT}}+B_{\text{ch},2}} \int_{f_{\text{ch},1}-f_{\text{CUT}}-B_{\text{ch},1}}^{f_{\text{ch},1}-f_{\text{CUT}}+B_{\text{ch},1}} \left| \sum_{n=0}^{N_p} p_n \cdot \int_0^L e^{j4\pi^2 f_1 f_2 \cdot \beta \cdot z} \cdot z^n \, dz \right|^2 df_1 df_2 \tag{39}$$

Then we apply the identical decomposition principle to the K_{MCI} integral. This allows us to express the complex core integral as a sum of real-valued integrals, with $I_{nm,\text{MCI}}$ terms combining two symmetric contributions and $I_{nn,\text{MCI}}$ terms representing the single

self-contribution. The corresponding real-valued integrals are:

$$I_{nm,\text{MCI}} = \int_{f_{\text{ch},2}-f_{\text{CUT}}-B_{\text{ch},2}}^{f_{\text{ch},2}-f_{\text{CUT}}+B_{\text{ch},2}} \int_{f_{\text{ch},1}-f_{\text{CUT}}-B_{\text{ch},1}}^{f_{\text{ch},1}-f_{\text{CUT}}+B_{\text{ch},1}} \int_0^L \int_0^L e^{j4\pi^2 f_1 f_2 \beta(z_1-z_2)} \cdot (z_1^n z_2^m + z_1^m z_2^n)\,\mathrm{d}z_1\,\mathrm{d}z_2\,\mathrm{d}f_1\,\mathrm{d}f_2 \tag{40}$$

$$I_{nn,\text{MCI}} = \int_{f_{\text{ch},2}-f_{\text{CUT}}-B_{\text{ch},2}}^{f_{\text{ch},2}-f_{\text{CUT}}+B_{\text{ch},2}} \int_{f_{\text{ch},1}-f_{\text{CUT}}-B_{\text{ch},1}}^{f_{\text{ch},1}-f_{\text{CUT}}+B_{\text{ch},1}} \int_0^L \int_0^L e^{j4\pi^2 f_1 f_2 \cdot \beta \cdot (z_1-z_2)} z_1^n z_2^n \, dz_1 dz_2 \, df_1 df_2 \tag{41}$$

And the final result is:

$$K_{\text{MCI}} = \sum_{n=0}^{N_p} \sum_{m=n+1}^{N_p} p_n p_m \cdot I_{nm,\text{MCI}} + \sum_{n=0}^{N_p} p_n^2 \cdot I_{nn,\text{MCI}} \tag{42}$$

We now have the integral expressions for the I_{nn} and I_{nm} terms for K_{SCI}, K_{XCI}, and K_{MCI}. Mathematica appears to be able to solve these integrals in closed-form (although special functions appear in the solution, which however we still consider "closed-form" anyway).

For most practical applications, a polynomial degree of $N_p = 5$ provides sufficient accuracy, with results that are almost indistinguishable from those obtained by direct numerical integration of the kernel. However, for challenging scenarios requiring very high reliability, such as profiles with ISRS or powerful Raman amplification, a higher-order approximation is necessary. It is found that a polynomial degree of $N_p = 9$ is needed to ensure accuracy [13]. As this paper aims to obtain the exact analytical solutions working for all contexts, we will raise the degree as close to 9 as possible.

After obtaining the closed-form solutions, our next steps are to: (1) explicitly evaluate and accumulate the I_{nm} and I_{nn} terms one by one, up to where it is practically possible, and (2) convert them into fast-executing software modules by translating them into `C` and then using the `Matlab` compiler to obtain `mex files`.

4 Solving for the Closed-Form Solution with Mathematica

4.1 Solving I_{nn} and I_{nm} for the SCI Kernel

For the K_{SCI} kernel, the integral expressions for I_{nn} and I_{nm}, see Eq. (33) and Eq. (34), are the simplest, as the integration limits with respect to f_1 and f_2 are the most basic. We

will therefore start with this case.

For the expression of I_{nn} and I_{nm}, we can directly input the complete four-fold integral into Mathematica. The software can solve for almost all the integral I_{nn} and I_{nm} required for the summation in Eq. (31) if we do not set N_p to a high value. Here, we refer to this approach as the **direct integral-solving method**. The corresponding Mathematica code is as follows (note that this code is now generalized to calculate any integral term. It handles the I_{nn} case (where $n = m$) and the I_{nm} case (where $n \neq m$) using a conditional `If` statement to select the appropriate integrand):

```
ClearAll["Global`*"];
n =  ; (* Set desired order n *)
m =  ; (* Set desired order m *)

B = Symbol["B"];
L = Symbol["L"];
β = Symbol["β"];

integrand =
  If[n == m, Exp[I*4*Pi^2*β*(z1 - z2)*f1*f2]*(z1^n*z2^n),
   Exp[I*4*Pi^2*β*(z1 - z2)*f1*f2]*(z1^n*z2^m + z1^m*z2^n)];

Inm = Integrate[
    Integrate[
        Integrate[
            Integrate[integrand, {z1, 0, L}], {z2, 0, L}], {f1,
   -B/2,
            B/2}], {f2, -B/2, B/2}];

Inm = FullSimplify[Inm,
    Assumptions → {B > 0, L > 0, β > 0}];

Inm
```

Even though the values of dispersion parameter β_2 can be either positive or negative, a key property of the obtained analytical solutions is their symmetry with respect to β_2. All derived formulas are even functions of β_2, meaning the result is independent of its sign. Therefore, we can use the absolute value of the dispersion in our calculations without any loss of generality. To ensure computational robustness and avoid potential implementation issues within mathematical software for negative-valued special function arguments, we

explicitly set the assumption $\beta_2 > 0$ throughout our symbolic calculations.

The **direct integral-solving method** attempts to compute the quadruple symbolic integral to find a closed-form analytical solution. However, due to the complex mathematical structure of the integrand, which involves a challenging combination of complex exponentials and polynomial terms, the difficulty of the problem often exceeds the capabilities of the symbolic integrator. For some certain (n, m) terms the program fails to find a closed-form solution and returns an expression that still contains the unevaluated `Integrate[...]` symbol. Figure 5 shows the solution status of all the I_{nn} and I_{nm} required for $N_p = 9$ using the **direct integral-solving method**.

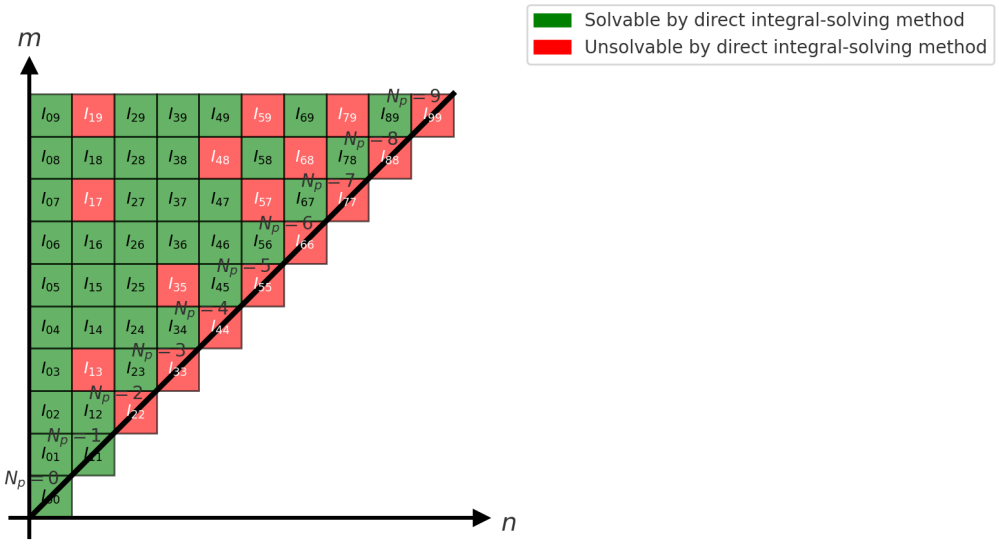

Figure 5: Solution status of direct integral-solving method.

At this point, we can use certain techniques to avoid such a heavy computational workload, for instance, by appropriately decomposing the integral expression. For the expression of I_{nn}, see Eq. (34), we begin by analyzing the integrand:

$$e^{j4\pi^2 f_1 f_2 \beta (z_1 - z_2)} \cdot z_1^n z_2^n$$

Using the property of exponential functions, it can be decomposed into a product of a function solely of z_1 and another solely of z_2:

$$(z_1^n \cdot e^{j4\pi^2 f_1 f_2 \beta z_1}) \cdot (z_2^n \cdot e^{-j4\pi^2 f_1 f_2 \beta z_2})$$

Based on this separation, the original nested double integral with respect to z_1 and z_2 is

transformed into a product of two independent single integrals:

$$\left(\int_0^L z_1^n e^{j4\pi^2 f_1 f_2 \beta z_1}\, dz_1\right) \cdot \left(\int_0^L z_2^n e^{-j4\pi^2 f_1 f_2 \beta z_2}\, dz_2\right)$$

Upon observing these two integrals, we can see they share the same mathematical structure. They can be represented by the general form:

$$\int_0^L z^n e^{i\alpha z}\, dz$$

where the parameter α is defined as $\alpha = \pm 4\pi^2 \cdot \beta \cdot f_1 \cdot f_2$.

For the expression of I_{nm}, we can use the same idea. First, we analyze the integrand (see Eq. (33)):

$$e^{j4\pi^2 f_1 f_2 \beta (z_1 - z_2)} \cdot (z_1^n z_2^m + z_1^m z_2^n)$$

We can split the integrand into two distinct parts:

$$(z_1^n e^{j4\pi^2 f_1 f_2 \beta z_1}) \cdot (z_2^m e^{-j4\pi^2 f_1 f_2 \beta z_2}) + (z_1^m e^{j4\pi^2 f_1 f_2 \beta z_1}) \cdot (z_2^n e^{-j4\pi^2 f_1 f_2 \beta z_2})$$

This transforms the double integral into a sum of two products of single, independent integrals:

$$\left(\int_0^L z_1^n e^{j4\pi^2 \beta f_1 f_2 z_1}\, dz_1\right) \cdot \left(\int_0^L z_2^m e^{-j4\pi^2 \beta f_1 f_2 z_2}\, dz_2\right) + \left(\int_0^L z_1^m e^{j4\pi^2 \beta f_1 f_2 z_1}\, dz_1\right) \cdot \left(\int_0^L z_2^n e^{-j4\pi^2 \beta f_1 f_2 z_2}\, dz_2\right)$$

Each of the four single-integral terms can be represented by the general form $\int_0^L z^k e^{i\alpha z}\, dz$.

Here, we refer to this approach as the **decomposing method**. The corresponding Mathematica code which handles both I_{nn} and I_{nm} case can be adapted as follows:

```
n =  ; (* Set desired order n *)
m =  ; (* Set desired order m *)

B = Symbol["B"];
L = Symbol["L"];
β = Symbol["β"];
$Assumptions = {B > 0, L > 0, β > 0};

F[k_, alpha_, L_] :=
  Integrate[z^k Exp[I alpha z], {z, 0, L},
```

```
   Assumptions → {L > 0, ∈[k, Integers],
     ∈[alpha, Reals]}];

integrand =
  If[n == m,
   F[n, 4 Pi^2 β f1 f2, L]*F[n, -4 Pi^2 β f1 f2, L],
   F[n, 4 Pi^2 β f1 f2, L]*F[m, -4 Pi^2 β f1 f2, L] +
    F[m, 4 Pi^2 β f1 f2, L]*F[n, -4 Pi^2 β f1 f2, L]];

Inm = Integrate[Integrate[integrand, {f1, -B/2, B/2}], {f2, -B
   /2, B/2}];

Inm = FullSimplify[Inm, Assumptions → $Assumptions];
Inm
```

However, a critical limitation arises when applying this method to integrals involving zeroth-order polynomial terms (I_{00} and I_{0m}). The issue stems from a removable singularity that appears in the analytical solution of the helper function $F[k, \alpha, L]$ specifically when $k = 0$.

For the case $k = 0$, the function F in the code above simplifies to:

$$F[0, \alpha, L] = \int_0^L e^{i\alpha z}\, dz = \frac{e^{i\alpha L} - 1}{i\alpha}$$

While this expression is valid for $\alpha \neq 0$, it becomes an indeterminate $0/0$ form at the singular point $\alpha = 0$. In the outer integration, the parameter $\alpha = 4\pi^2\beta f_1 f_2$ is zero whenever $f_1 = 0$ or $f_2 = 0$. Since the integration domain for SCI includes these points, Mathematica is tasked with integrating a function that contains a singularity. This is a computationally challenging task that often fails, leading to an unevaluated integral or an error.

Therefore, while the decomposing method is highly efficient for higher degree cases, it is not robust for cases involving zeroth-order terms due to this singularity. Fortunately, the **direct integral-solving method** of solving the original four-fold integral can successfully compute I_{00} as well as all the I_{0m} terms required for the $N_p = 9$ case.

Here is an example of I_{11} result:

$$I_{11} = \frac{1}{9B^6\pi^8\beta^4}\left(2 + 9B^4L^2\pi^4\beta^2\right.$$

$$
\begin{aligned}
&- 2\left(1 + 4B^4L^2\pi^4\beta^2\right)\cos\left(B^2L\pi^2\beta\right) \\
&- 2B^2L\pi^2\beta\sin\left(B^2L\pi^2\beta\right) \\
&+ 2B^6L^3\pi^6\beta^3\left[3B^2L\pi^2\beta\,{}_2F_3\left(\frac{1}{2},\frac{1}{2};\frac{3}{2},\frac{3}{2},\frac{3}{2};-\frac{1}{4}B^4L^2\pi^4\beta^2\right)\right. \\
&\quad \left.-4\mathrm{Si}\left(B^2L\pi^2\beta\right)\right]\Bigg)
\end{aligned}
$$

The terms $\mathrm{Si}(x)$ and ${}_2F_3(\dots)$ that appear in the solution are standard special functions. $\mathrm{Si}(x)$ is the Sine Integral function, and ${}_2F_3$ is the generalized hypergeometric function. Now let us review this result with reference to Eq. (19). The correspondence of the parameters is as follows:

$$
\begin{aligned}
B &= B_{\text{CUT}} \\
L &= L_s^{(n_s)} \\
\beta &= \beta_{\text{2eff,CUT}}^{(n_s)}
\end{aligned}
$$

Additionally, several functions and special functions appear frequently in the results we obtain, making it sensible to define a more compact notation for them:

$$
\begin{aligned}
\mathrm{S} &= \sin\left(B^2L\pi^2\beta\right) \\
\mathrm{C} &= \cos\left(B^2L\pi^2\beta\right) \\
\mathrm{SI} &= \mathrm{Si}\left(B^2L\pi^2\beta\right) \\
\mathrm{H} &= {}_2F_3\left(\frac{1}{2},\frac{1}{2};\frac{3}{2},\frac{3}{2},\frac{3}{2};-\frac{1}{4}B^4L^2\pi^4\beta^2\right)
\end{aligned}
$$

Here are the results for the kernel integrals for SCI, for $N_p = 0, 1, 2, 3$:

For the case $N_p = 0$:

$$
\begin{aligned}
K_{\text{SCI,CUT}}^{(n_s)}\Big|_{N_p=0} &= \int_{-B_{\text{CUT}}/2}^{B_{\text{CUT}}/2}\int_{-B_{\text{CUT}}/2}^{B_{\text{CUT}}/2}\left|\int_0^{L_s^{(n_s)}} e^{j4\pi^2 f_1' f_2' \beta_{\text{2eff,CUT}}^{(n_s)} z}\cdot p_{0,\text{CUT}}^{(n_s)}\,dz\right|^2 df_1' df_2' \\
&= p_0^2\cdot I_{00} \\
&= p_0^2\cdot\left[-\frac{2\left(\pi^2\beta B^2L\left(\mathrm{SI}-\pi^2\beta B^2L\beta H\right)+C-1\right)}{\pi^4\beta^2B^2}\right]
\end{aligned}
$$

For the case $N_p = 1$:

$$
K_{\text{SCI,CUT}}^{(n_s)}\Big|_{N_p=1} = \int_{-B_{\text{CUT}}/2}^{B_{\text{CUT}}/2}\int_{-B_{\text{CUT}}/2}^{B_{\text{CUT}}/2}
$$

$$
\begin{aligned}
&\cdot \left| \int_0^{L_s^{(n_s)}} e^{j4\pi^2 f_1' f_2' \beta_{\text{2eff,CUT}}^{(n_s)} z} \cdot \left(p_{0,\text{CUT}}^{(n_s)} + p_{1,\text{CUT}}^{(n_s)} \cdot z \right) \mathrm{d}z \right|^2 \mathrm{d}f_1' \mathrm{d}f_2' \\
&= p_0^2 \cdot I_{00} + p_0 p_1 \cdot I_{01} + p_1^2 \cdot I_{11} \\
&= p_0^2 \cdot \left[- \frac{2\left(\pi^2 \beta B^2 L \left(\mathrm{SI} - \pi^2 \beta B^2 L \beta \mathrm{H}\right) + \mathrm{C} - 1\right)}{\pi^4 \beta^2 B^2} \right] \\
&\quad + p_0 p_1 \cdot \left[\frac{2L\left(\pi^2 \beta B^2 L \left(\pi^2 \beta B^2 L \beta \mathrm{H} - \mathrm{SI}\right) - \mathrm{C} + 1\right)}{\pi^4 \beta^2 B^2} \right] \\
&\quad + p_1^2 \cdot \left[\frac{1}{9\pi^8 \beta^4 B^6} \Big(2\pi^6 \beta^3 B^6 L^3 \left(3\pi^2 \beta B^2 L \mathrm{H} - 4\,\mathrm{SI} \right) \right. \\
&\qquad\qquad + 9\pi^4 \beta^2 B^4 L^2 - 2\pi^2 \beta B^2 L \mathrm{S} \\
&\qquad\qquad \left. - 2\left(4\pi^4 \beta^2 B^4 L^2 + 1\right) \mathrm{C} + 2 \Big) \right]
\end{aligned}
$$

For the case $N_p = 2$:

$$
\begin{aligned}
K_{\text{SCI,CUT}}^{(n_s)}\Big|_{N_p=2} &= \int_{-B_{\text{CUT}}/2}^{B_{\text{CUT}}/2} \int_{-B_{\text{CUT}}/2}^{B_{\text{CUT}}/2} \left| \int_0^{L_s^{(n_s)}} e^{j4\pi^2 f_1' f_2' \beta_{\text{2eff,CUT}}^{(n_s)} z} \cdot \left[\sum_{n=0}^{2} p_{n,\text{CUT}}^{(n_s)} \cdot z^n \right] dz \right|^2 df_1' df_2' \\
&= p_0^2 \cdot I_{00} + p_0 p_1 \cdot I_{01} + p_1^2 \cdot I_{11} + p_0 p_2 \cdot I_{02} + p_1 p_2 \cdot I_{12} + p_2^2 \cdot I_{22} \\
&= p_0^2 \cdot \left[- \frac{2\left(\pi^2 \beta B^2 L \left(\mathrm{SI} - \pi^2 \beta B^2 L \beta \mathrm{H}\right) + \mathrm{C} - 1\right)}{\pi^4 \beta^2 B^2} \right] \\
&\quad + p_0 p_1 \cdot \left[\frac{2L\left(\pi^2 \beta B^2 L \left(\pi^2 \beta B^2 L \beta \mathrm{H} - \mathrm{SI}\right) - \mathrm{C} + 1\right)}{\pi^4 \beta^2 B^2} \right] \\
&\quad + p_1^2 \cdot \left[\frac{1}{9\pi^8 \beta^4 B^6} \Big(2\pi^6 \beta^3 B^6 L^3 \left(3\pi^2 \beta B^2 L \mathrm{H} - 4\,\mathrm{SI} \right) \right. \\
&\qquad\qquad + 9\pi^4 \beta^2 B^4 L^2 - 2\pi^2 \beta B^2 L \mathrm{S} \\
&\qquad\qquad \left. - 2\left(4\pi^4 \beta^2 B^4 L^2 + 1\right) \mathrm{C} + 2 \Big) \right] \\
&\quad + p_0 p_2 \cdot \left[\frac{1}{9\pi^8 \beta^4 B^6} \Big(\pi^6 \beta^3 B^6 L^3 \left(12\pi^2 \beta B^2 L \mathrm{H} - 13\mathrm{SI} \right) \right. \\
&\qquad\qquad + 18\pi^4 \beta^2 B^4 L^2 - \pi^2 \beta B^2 L \mathrm{S} \\
&\qquad\qquad \left. + \left(8 - 13\pi^4 \beta^2 B^4 L^2\right) \mathrm{C} - 8 \Big) \right] \\
&\quad + p_1 p_2 \cdot \left[\frac{L^2}{2\pi^6 \beta^3 B^4} \Big(\pi^4 \beta^2 B^4 L^2 \left(2\pi^2 \beta B^2 L \mathrm{H} - 3\mathrm{SI} \right) \right.
\end{aligned}
$$

$$
\begin{aligned}
&\qquad\qquad - \mathrm{S} + \pi^2\beta B^2 L\left(4 - 3\mathrm{C}\right)\Big)\Bigg] \\
&+ p_2^2 \cdot \Bigg[\frac{1}{25\pi^{12}\beta^6 B^{10}}\Big(\pi^{10}\beta^5 B^{10} L^5\left(10\pi^2\beta B^2 L\mathrm{H} - 17\mathrm{SI}\right) \\
&\qquad\qquad - \pi^2\beta B^2 L\left(7\pi^4\beta^2 B^4 L^2 + 8\right)\mathrm{S} \\
&\qquad\qquad + \left(-17\pi^8\beta^4 B^8 L^4 + 4\pi^4\beta^2 B^4 L^2 - 8\right)\mathrm{C} \\
&\qquad\qquad + 25\pi^8\beta^4 B^8 L^4 + 8\Big)\Bigg]
\end{aligned}
$$

For the case $N_p = 3$:

$$
\begin{aligned}
K_{\mathrm{SCI,CUT}}^{(n_s)}\Big|_{N_p=3} &= \int_{-B_{\mathrm{CUT}}/2}^{B_{\mathrm{CUT}}/2}\int_{-B_{\mathrm{CUT}}/2}^{B_{\mathrm{CUT}}/2}\left|\int_0^{L_s^{(n_s)}} e^{j4\pi^2 f_1' f_2' \beta_{\mathrm{2eff,CUT}}^{(n_s)} z}\cdot\left[\sum_{n=0}^{3} p_{n,\mathrm{CUT}}^{(n_s)}\cdot z^n\right] dz\right|^2 df_1' df_2' \\
&= p_0^2\cdot I_{00} + p_0p_1\cdot I_{01} + p_1^2\cdot I_{11} + p_0p_2\cdot I_{02} + p_1p_2\cdot I_{12} + p_2^2\cdot I_{22} \\
&\quad + p_0p_3\cdot I_{03} + p_1p_3\cdot I_{13} + p_2p_3\cdot I_{23} + p_3^2\cdot I_{33} \\
&= p_0^2\cdot\Bigg[-\frac{2\left(\pi^2\beta B^2 L\left(\mathrm{SI} - \pi^2\beta B^2 L\beta\mathrm{H}\right) + \mathrm{C} - 1\right)}{\pi^4\beta^2 B^2}\Bigg] \\
&\quad + p_0p_1\cdot\Bigg[\frac{2L\left(\pi^2\beta B^2 L\left(\pi^2\beta B^2 L\beta\mathrm{H} - \mathrm{SI}\right) - \mathrm{C} + 1\right)}{\pi^4\beta^2 B^2}\Bigg] \\
&\quad + p_1^2\cdot\Bigg[\frac{1}{9\pi^8\beta^4 B^6}\Big(2\pi^6\beta^3 B^6 L^3\left(3\pi^2\beta B^2 L\mathrm{H} - 4\,\mathrm{SI}\right) \\
&\qquad\qquad + 9\pi^4\beta^2 B^4 L^2 - 2\pi^2\beta B^2 L\mathrm{S} \\
&\qquad\qquad - 2\left(4\pi^4\beta^2 B^4 L^2 + 1\right)\mathrm{C} + 2\Big)\Bigg] \\
&\quad + p_0p_2\cdot\Bigg[\frac{1}{9\pi^8\beta^4 B^6}\Big(\pi^6\beta^3 B^6 L^3\left(12\pi^2\beta B^2 L\mathrm{H} - 13\mathrm{SI}\right) \\
&\qquad\qquad + 18\pi^4\beta^2 B^4 L^2 - \pi^2\beta B^2 L\mathrm{S} \\
&\qquad\qquad + \left(8 - 13\pi^4\beta^2 B^4 L^2\right)\mathrm{C} - 8\Big)\Bigg] \\
&\quad + p_1p_2\cdot\Bigg[\frac{L^2}{2\pi^6\beta^3 B^4}\Big(\pi^4\beta^2 B^4 L^2\left(2\pi^2\beta B^2 L\mathrm{H} - 3\mathrm{SI}\right) \\
&\qquad\qquad - \mathrm{S} + \pi^2\beta B^2 L\left(4 - 3\mathrm{C}\right)\Big)\Bigg]
\end{aligned}
$$

$$
\begin{aligned}
&+ p_2^2 \cdot \Bigg[\frac{1}{25\pi^{12}\beta^6 B^{10}} \Big(\pi^{10}\beta^5 B^{10} L^5 \left(10\pi^2 \beta B^2 L \mathrm{H} - 17\mathrm{SI}\right) \\
&\qquad - \pi^2 \beta B^2 L \left(7\pi^4 \beta^2 B^4 L^2 + 8\right) \mathrm{S} \\
&\qquad + \left(-17\pi^8 \beta^4 B^8 L^4 + 4\pi^4 \beta^2 B^4 L^2 - 8\right) \mathrm{C} \\
&\qquad + 25\pi^8 \beta^4 B^8 L^4 + 8 \Big) \Bigg] \\
&+ p_0 p_3 \cdot \Bigg[\frac{L}{6\pi^8 \beta^4 B^6} \Big(\pi^6 \beta^3 B^6 L^3 \left(6\pi^2 \beta B^2 L \mathrm{H} - 7\mathrm{SI}\right) \\
&\qquad + 12\pi^4 \beta^2 B^4 L^2 - \pi^2 \beta B^2 L \mathrm{S} \\
&\qquad + \left(8 - 7\pi^4 \beta^2 B^4 L^2\right) \mathrm{C} - 8 \Big) \Bigg] \\
&+ p_1 p_3 \cdot \Bigg[\frac{1}{75\pi^{12}\beta^6 B^{10}} \Big(\pi^{10}\beta^5 B^{10} L^5 \left(60\pi^2 \beta B^2 L \mathrm{H} - 97\mathrm{SI}\right) \\
&\qquad + \pi^2 \beta B^2 L \left(72 - 37\pi^4 \beta^2 B^4 L^2\right) \mathrm{S} \\
&\qquad + \left(-97\pi^8 \beta^4 B^8 L^4 + 14\pi^4 \beta^2 B^4 L^2 + 72\right) \mathrm{C} \\
&\qquad + 150\pi^8 \beta^4 B^8 L^4 - 50\pi^4 \beta^2 B^4 L^2 - 72 \Big) \Bigg] \\
&+ p_2 p_3 \cdot \Bigg[\frac{L^3}{9\pi^8 \beta^4 B^6} \Big(\pi^6 \beta^3 B^6 L^3 \left(6\pi^2 \beta B^2 L \mathrm{H} - 11\mathrm{SI}\right) \\
&\qquad + 18\pi^4 \beta^2 B^4 L^2 - 5\pi^2 \beta B^2 L \mathrm{S} \\
&\qquad + \left(4 - 11\pi^4 \beta^2 B^4 L^2\right) \mathrm{C} - 4 \Big) \Bigg] \\
&+ p_3^2 \cdot \Bigg[\frac{1}{147\pi^{16}\beta^8 B^{14}} \Bigg(\pi^{14}\beta^7 B^{14} L^7 \left(42\pi^2 \beta B^2 L \mathrm{H} - 83\mathrm{SI}\right) \\
&\qquad + \pi^2 \beta B^2 L \left(-41\pi^8 \beta^4 B^8 L^4 + 36\pi^4 \beta^2 B^4 L^2 - 216\right) \mathrm{S} \\
&\qquad + \Big(\pi^4 \beta^2 B^4 L^2 \left(-83\pi^8 \beta^4 B^8 L^4 + 40\pi^4 \beta^2 B^4 L^2 + 108\right) \\
&\qquad\quad -216 \Big) \mathrm{C} \\
&\qquad + 49\pi^8 \beta^4 B^8 L^4 \left(3\pi^4 \beta^2 B^4 L^2 - 1\right) + 216 \Bigg) \Bigg]
\end{aligned}
$$

Note that to simplify the notation, we replace the term $p_{n,\mathrm{CUT}}^{(n_s)}$ with the shorthand p_n for any generic index $n = 0, 1, 2, \ldots$. For example, $p_{0,\mathrm{CUT}}^{(n_s)}$ is written as p_0, and $p_{1,\mathrm{CUT}}^{(n_s)}$ is written as p_1, and so on.

By utilizing both the **direct integral-solving method** and the **decomposing method** in Mathematica, we can obtain the analytical expressions of all I_{nn} and I_{nm} required for $N_p = 9$. Regardless of the value of N_p, what we need to do is simply multiply these analytical solutions by the corresponding polynomial coefficients and then sum them up according to Eq. (31). This summation structure confirms a crucial characteristic of the SCI kernel solution: reusability. When increasing the polynomial degree from N_{p-1} to N_p, the entire analytical result obtained for N_{p-1} is preserved. The solution for N_p is then generated by only appending the new set of I_{nm} and I_{nn} multiplied by their corresponding polynomial coefficients.

Here we present the solution as a weighted sum of the fundamental integral terms (e.g., $p_0^2 \cdot I_{00} + p_1^2 \cdot I_{11} + p_0 p_1 \cdot I_{01}$). This structure is intentionally mirrored in our C/MEX code, where each unique integral ($I_{00}, I_{01}, \dots$) is implemented as a distinct function. This modular approach was chosen for a practical advantage: it greatly facilitates debugging and verification. The output of each individual function in the code can be independently tested and validated against its corresponding symbolic solution from Mathematica, a process which is tough with a single, fully expanded formula. This ensures a one-to-one correspondence between the mathematical derivation and the final software implementation, guaranteeing accuracy and making the code easier to maintain.

To validate the series of derivations of the K_{SCI} expression presented in Section 3.1, as well as the feasibility of the associated Mathematica code, we need to test our results for $N_p = 3, 5, 7, 9$ against the result of directly executing numerical integration to Eq. (19) at $N_p = 9$. After extensive testing, the results indicate that our entire derivation process for K_{SCI} is correct and yields a highly accurate result. Here, we demonstrate the test results for one channel exhibiting a relatively complex SPP. The comparison between exact SPP and polynomial fit with $N_p = 3, 5, 7, 9$ for the test channel is shown in Figure 6, and we can observe that the fitting accuracy improves as the polynomial degree increases.

- **Fiber Length (L):** 100 km
- **Dispersion (β_2):** 20.41826538 ps^2/km
- **CUT Bandwidth ($B_{\mathbf{CUT}}$):** 100 GHz
- **Polynomial Power Profile Coefficients.**
  - $N_p = 3$ (p_0 to p_3): [0.90316, -1.8690e-05, -7.0873e-11, 2.5193e-15]
  - $N_p = 5$ (p_0 to p_5): [0.97238, -2.1831e-05, -7.3546e-10, 3.7936e-14, -5.5316e-19, 2.7072e-24]

- $N_p = 7$ (p_0 to p_7): [0.99128, -2.4910e-05, -1.1162e-09, 9.4561e-14, -2.9086e-18, 4.6200e-23, -3.7257e-28, 1.2075e-33]
- $N_p = 9$ (p_0 to p_9): [0.99782, -2.8281e-05, -8.4022e-10, 1.0528e-13, -4.9400e-18, 1.3932e-22, -2.4481e-27, 2.6025e-32, -1.5285e-37, 3.8112e-43]

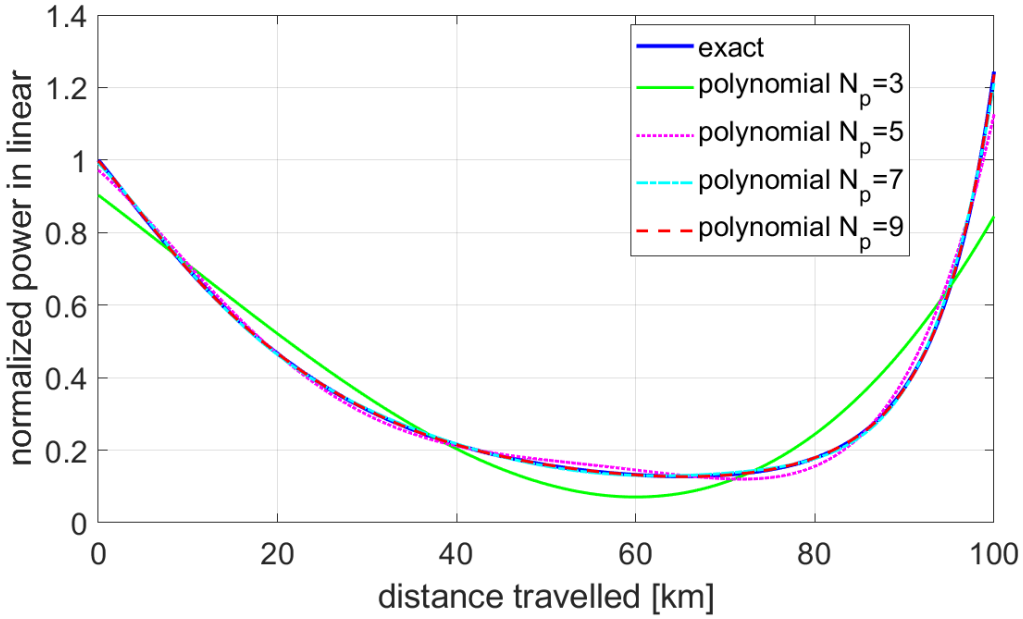

Figure 6: Polynomial representation of the normalized SPPs along the 100 km fiber for the channel chosen: The blue solid curve is the exact SPP, and the remaining curves are the polynomial fits with $N_p = 3, 5, 7, 9$.

The results in Table 1 demonstrate excellent convergence behavior: as the polynomial order increases, the analytical solution rapidly approaches the reference value. The convergence is near-perfect at the highest order, where the relative error drops to 0.00000% at $N_p = 9$. This high level of precision confirms that the closed-form expression accurately models the Self-Channel Interference.

Table 1: Comparison between analytical solution and numerical integration

N_p	K_{SCI} **(Analytical Solution)**	**Speed**	K_{SCI} **(Numerical Integration)**	**Speed**	**Relative Error (Absolute)**
3	6.200689573	0.0945s	7.56265856	64.3077s	18.00913%
5	7.18623079	0.0957s			4.97745%
7	7.466336976	0.0951s			1.27365%
9	7.562658546	0.0974s			0.00000%

Furthermore, the comparison highlights a dramatic advantage in computational efficiency. Although the numerical integration required 64.3077s to compute the reference value, the

analytical solution consistently calculates the K_{SCI} value instantaneously across all orders, with computation times around 0.095s. This difference demonstrates that the closed-form expression reduces the computation time by ~ 3 orders of magnitude, proving the analytical solution is a highly efficient tool for real-time performance monitoring and system design.

Since the series of derivations of the K_{SCI} expression presented in Section 3.1, as well as the feasibility of the associated Mathematica code, are confirmed to be sound and viable. Consequently, these successful foundational results allow us to confidently apply the same derivation methodology to extend the analytical solutions for the K_{XCI} and K_{MCI} in subsequent work.

4.2 Generalized Solution for all Kernels

For K_{XCI} and K_{MCI}, the integral expressions become significantly more complex than the K_{SCI} case. Although the integrand remains unchanged, the frequency integration limits introduce additional parameters. Especially in the case of K_{MCI}, it contains the highest number of independent parameters in its integration limits. The drawback is that more parameters increase computational complexity and the length of the analytical solution, complicating the final compilation stage. To solve this problem efficiently, we can introduce a generalized form for the kernel integrals. This approach allows us to solve the most complex case (MCI) once, and then derive the results for the simpler XCI and SCI cases by direct parameter substitution.

The generalized solution must adhere to the decomposition principle established in Section 3, where cross-terms ($n \neq m$) are formed by summing two symmetric contributions and self-terms ($n = m$) contain only a single contribution. Therefore, we define two distinct generalized functions, $I_{nm,\text{gen}}$ and $I_{nn,\text{gen}}$, to maintain this necessary conceptual and structural distinction.

The generalized integral uses four symbolic placeholders, a, b, c, and d. We set the limits for the inner integral (over f_1) be $[a, b]$ and the limits for the outer integral (over f_2) be $[c, d]$.

Let us define the general solution:

$$I_{nm,\text{gen}} = \int_c^d \int_a^b \int_0^L \int_0^L e^{j4\pi^2 f_1 f_2 \cdot \beta \cdot (z_1 - z_2)} \cdot (z_1^n z_2^m + z_1^m z_2^n)\, dz_1 dz_2\, df_1 df_2 \quad (\text{For } n \neq m) \tag{43}$$

$$I_{nn,\text{gen}} = \int_c^d \int_a^b \int_0^L \int_0^L e^{j4\pi^2 f_1 f_2 \cdot \beta \cdot (z_1 - z_2)} \cdot z_1^n z_2^n\, dz_1 dz_2\, df_1 df_2 \quad (\text{For } n = m) \tag{44}$$

The final general kernel is then expressed using both terms:

$$K_{\text{gen}} = \sum_{n=0}^{N_p} \sum_{m=n+1}^{N_p} p_n p_m \cdot I_{nm,\text{gen}} + \sum_{n=0}^{N_p} p_n^2 \cdot I_{nn,\text{gen}} \tag{43}$$

The strategy is to first derive the closed-form solution for both $I_{nm,\text{gen}}$ and $I_{nn,\text{gen}}$ using the symbolic placeholders a, b, c, and d so that we can obtain the K_{gen}. The specific results for the MCI, XCI, and SCI kernels are then obtained by substituting the corresponding physical limits directly into the final closed-form algebraic expression for the generalized solution. And then use the Eq. (12), Eq. (14) and Eq. (16) we can have the corresponding NLI PSD.

Application to MCI Kernel: The MCI kernel has asymmetric integration limits over f_1 and f_2. The parameters for the MCI case are mapped as follows, where $B_{\text{ch},1}$ and $B_{\text{ch},2}$ are the bandwidths of the two mixing channels ($f_{\text{ch},1}$ and $f_{\text{ch},2}$):

- $a = f_{\text{ch},1} - f_{\text{CUT}} - B_{\text{ch},1}/2$
- $b = f_{\text{ch},1} - f_{\text{CUT}} + B_{\text{ch},1}/2$
- $c = f_{\text{ch},2} - f_{\text{CUT}} - B_{\text{ch},2}/2$
- $d = f_{\text{ch},2} - f_{\text{CUT}} + B_{\text{ch},2}/2$

Application to XCI Kernel: The solution for the K_{XCI} can be derived from the general solution by applying symmetry constraints to the limits. For the horizontal axis XCI case, the limits of the outer integral (over f_2) are symmetric around zero. We substitute the following specific values into $I_{nm,\text{gen}}$ and $I_{nn,\text{gen}}$:

- $a = f_{\text{ch}} - f_{\text{CUT}} - B_{\text{ch}}/2$
- $b = f_{\text{ch}} - f_{\text{CUT}} + B_{\text{ch}}/2$
- $c = -B_{\text{CUT}}/2$
- $d = B_{\text{CUT}}/2$

Application to SCI Kernel: The simplest case, the K_{SCI} can also be derived from this same general solution. Here, both integration limits are symmetric and identical to the bandwidth of the channel under test:

- $a = -B_{\text{CUT}}/2$
- $b = B_{\text{CUT}}/2$
- $c = -B_{\text{CUT}}/2$

- $d = B_{\text{CUT}}/2$

However, still the general form of the integral represents a substantial increase in complexity compared to the cases discussed in Section 4.1. Consequently, neither executing the **direct integral-solving method** nor the **decomposing method** is viable for solving high-degree cases, necessitating a more robust methodology.

The starting point for our analysis is the general integral form $I_{nm,\text{gen}}$. We begin by using Euler's formula, $e^{j\theta} = \cos(\theta) + j\sin(\theta)$, to expand the complex exponential term in the integrand. Let $\theta = 4\pi^2 f_1 f_2 \beta(z_1 - z_2)$. The integrand becomes:

$$[\cos(\theta) + j\sin(\theta)] \cdot (z_1^n z_2^m + z_1^m z_2^n)$$

Distributing the terms, the integral can be split into its real and imaginary parts:

$$\begin{aligned} I_{nm,\text{gen}} = &\int_c^d \int_a^b \int_0^L \int_0^L \cos(\theta)(z_1^n z_2^m + z_1^m z_2^n)\, dz_1 dz_2\, df_1 df_2 \\ &+ j \int_c^d \int_a^b \int_0^L \int_0^L \sin(\theta)(z_1^n z_2^m + z_1^m z_2^n)\, dz_1 dz_2\, df_1 df_2 \end{aligned}$$

As we mentioned above that all of the integrals $I_{nn,\text{gen}}$ and $I_{nm,\text{gen}}$ are real, so the entire four-fold integral of the imaginary (sine) part can be seen as zero.

$$\int_c^d \int_a^b \int_0^L \int_0^L \sin\left(4\pi^2 f_1 f_2 \beta(z_1 - z_2)\right)(z_1^n z_2^m + z_1^m z_2^n)\, dz_1 dz_2\, df_1 df_2 = 0$$

Then the value of $I_{nm,gen}$ is determined entirely by its real part (the cosine integral). We can therefore write the final, simplified expression for computation:

$$I_{nm,\text{gen}} = \int_c^d \int_a^b \int_0^L \int_0^L \cos\left(4\pi^2 f_1 f_2 \beta(z_1 - z_2)\right)(z_1^n z_2^m + z_1^m z_2^n)\, dz_1 dz_2\, df_1 df_2$$

This transformation is the key to solving the problem efficiently in Mathematica. Asking the symbolic engine to solve an integral with a purely real 'Cos' function is computationally more direct and stable than working with a complex 'Exp' function throughout the entire derivation.

The derivation for the $I_{nn,\text{gen}}$ integrals follows the same procedure as for $I_{nm,\text{gen}}$. The corresponding real-valued expression for computation is therefore:

$$I_{nn,\text{gen}} = \int_c^d \int_a^b \int_0^L \int_0^L \cos\left(4\pi^2 f_1 f_2 \beta(z_1 - z_2)\right) \cdot (z_1^n z_2^n)\, dz_1 dz_2\, df_1 df_2$$

This method can be referred as **cosine method**. The Mathematica code which handles both $I_{nn,\text{gen}}$ (where $n = m$) and the $I_{nm,\text{gen}}$ case (where $n \neq m$) using a conditional `If` statement is as follows:

```
n =  ; (* Set desired order n *)
m =  ; (* Set desired order m *)

L = Symbol["L"];
β = Symbol["β"];
a = Symbol["a"];
b = Symbol["b"];
c = Symbol["c"];
d = Symbol["d"];

$Assumptions = {L > 0, β > 0, a \[∈] Reals,
    b \[∈] Reals, c \[∈] Reals, d \[∈] Reals};

integrandZ[f1_, f2_] :=
  Module[{alpha = 4 Pi^2 β f1 f2, integrand},
   integrand =
    If[n == m, Cos[alpha*(z1 - z2)]*(z1^n*z2^n),
     Cos[alpha*(z1 - z2)]*(z1^n*z2^m + z1^m*z2^n)];
   Integrate[Integrate[integrand, {z1, 0, L}], {z2, 0, L}]];

Inm = Integrate[integrandZ[f1, f2], {f2, c, d}, {f1, a, b},
    Assumptions → $Assumptions, GenerateConditions → False];

Inm = Collect[Together[Inm], {Pi, β}, Simplify];

Inm
```

A specific limitation of the **cosine method** was observed during its application. The method successfully yields the analytical solutions for all the $I_{nm,\text{gen}}$ and $I_{nm,\text{gen}}$ required for $N_p = 9$ but $I_{04,\text{gen}}$, $I_{06,\text{gen}}$ and $I_{08,\text{gen}}$ (see Figure 7).

The reason for this specific pattern of failure is not a simple question of parity, but rather a critical threshold of symbolic complexity in the intermediate expression that is passed to the final integrator.

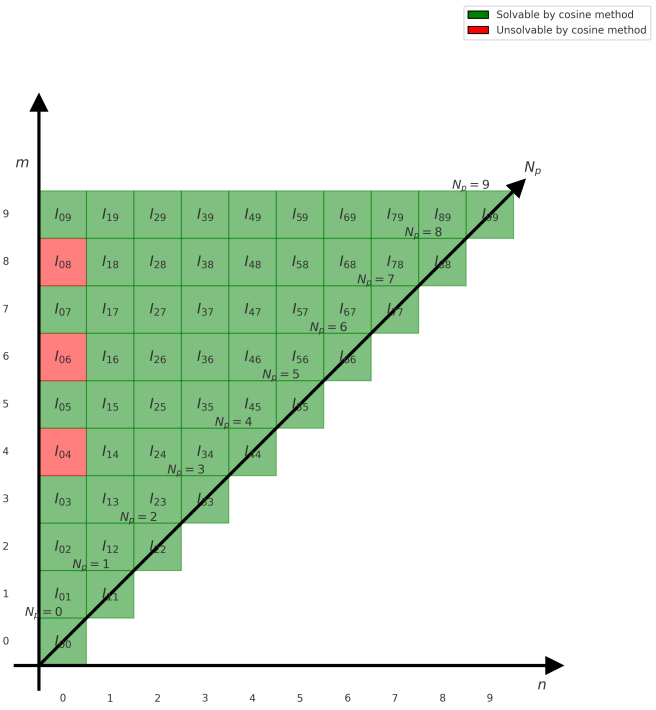

Figure 7: The inability to solve for $I_{04,\text{gen}}$, $I_{06,\text{gen}}$ and $I_{08,\text{gen}}$ means that we could only achieve a maximum polynomial degree of $N_p = 3$, which is not enough in accuracy.

Therefore, we can only attempt alternative methods. As mentioned earlier, the **decomposing method** is not applicable to I_{0m} cases, leaving the **direct integral-solving method** as the only viable approach at this stage. However, due to the lack of computational efficiency and optimization in this method, it can only provide solutions for $I_{04,\text{gen}}$ and $I_{06,\text{gen}}$, but not for $I_{08,\text{gen}}$.

This means that, until a better method is found, we are only able to derive all $I_{nn,\text{gen}}$ and $I_{nm,\text{gen}}$ required for $N_p = 7$ (see Figure 8). It is unfortunate, as we are just one term away ($I_{08,\text{gen}}$) from completing the case of $N_p = 9$. However, for the context of this work and practical NLI calculations, $N_p = 7$ is more than sufficient. Consequently, we will fix $N_p = 7$ for all subsequent simulation comparisons and analysis. The goal of completing the full analytical solution for $N_p = 9$ will be addressed in future work.

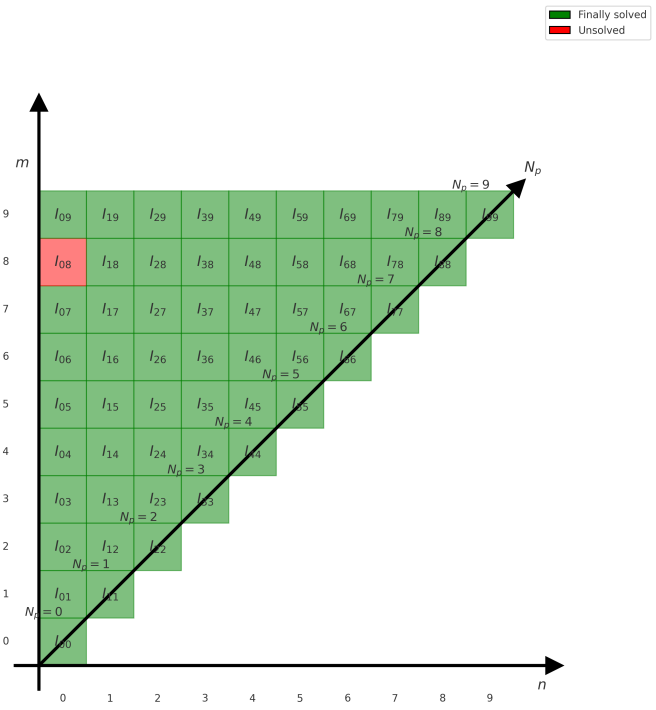

Figure 8: Now that $I_{04,\text{gen}}$ and $I_{06,\text{gen}}$ has been solved, we can implement the model up to $N_p = 7$.

Here is an example of $I_{11,\text{gen}}$ result:

$$
\begin{aligned}
I_{11,\text{gen}} = \frac{L^4}{3}\Bigg(&2ac\,{}_2F_3\left(\frac{1}{2},\frac{1}{2};\frac{3}{2},\frac{3}{2},\frac{3}{2};-4a^2c^2L^2\pi^4\beta^2\right)\\
&-2ad\,{}_2F_3\left(\frac{1}{2},\frac{1}{2};\frac{3}{2},\frac{3}{2},\frac{3}{2};-4a^2d^2L^2\pi^4\beta^2\right)\\
&-2bc\,{}_2F_3\left(\frac{1}{2},\frac{1}{2};\frac{3}{2},\frac{3}{2},\frac{3}{2};-4b^2c^2L^2\pi^4\beta^2\right)\\
&+2bd\,{}_2F_3\left(\frac{1}{2},\frac{1}{2};\frac{3}{2},\frac{3}{2},\frac{3}{2};-4b^2d^2L^2\pi^4\beta^2\right)\Bigg)\\
&+\frac{L^2}{144\pi^4ab\beta^2cd}\Big(8bc\cos\left(4\pi^2a\beta dL\right)-8ac\cos\left(4\pi^2b\beta dL\right)\\
&\qquad-8bd\cos\left(4\pi^2a\beta cL\right)+8ad\cos\left(4\pi^2b\beta cL\right)\\
&\qquad+9ac-9ad-9bc+9bd\Big)\\
&-\frac{2L^3}{9\pi^2\beta}\Big(\text{Si}\left(4acL\pi^2\beta\right)-\text{Si}\left(4adL\pi^2\beta\right)-\text{Si}\left(4bcL\pi^2\beta\right)+\text{Si}\left(4bdL\pi^2\beta\right)\Big)\\
&+\frac{L}{288\pi^6a^2b^2\beta^3c^2d^2}\Big(c^2\left(b^2\sin\left(4\pi^2a\beta dL\right)-a^2\sin\left(4\pi^2b\beta dL\right)\right)\\
&\qquad+a^2d^2\sin\left(4\pi^2b\beta cL\right)-b^2d^2\sin\left(4\pi^2a\beta cL\right)\Big)
\end{aligned}
$$

$$+\frac{1}{1152\pi^8 a^3b^3\beta^4c^3d^3}\Big(-a^3c^3\cos\Big(4\pi^2 b\beta dL\Big)+a^3d^3\cos\Big(4\pi^2 b\beta cL\Big)$$
$$+a^3c^3-a^3d^3+b^3c^3\cos\Big(4\pi^2 a\beta dL\Big)$$
$$-b^3d^3\cos\Big(4\pi^2 a\beta cL\Big)-b^3c^3+b^3d^3\Big)$$

Several functions and special functions appear frequently in the results we obtain, making it sensible to define a more compact notation for them:

$$\begin{aligned}
C_{ac}&=\cos(4\pi^2 a\beta cL) & S_{ac}&=\sin(4\pi^2 a\beta cL) & \mathbf{SI}_{ac}&=\mathrm{Si}(4\pi^2 a\beta cL)\\
C_{ad}&=\cos(4\pi^2 a\beta dL) & S_{ad}&=\sin(4\pi^2 a\beta dL) & \mathbf{SI}_{ad}&=\mathrm{Si}(4\pi^2 a\beta dL)\\
C_{bc}&=\cos(4\pi^2 b\beta cL) & S_{bc}&=\sin(4\pi^2 b\beta cL) & \mathbf{SI}_{bc}&=\mathrm{Si}(4\pi^2 b\beta cL)\\
C_{bd}&=\cos(4\pi^2 b\beta dL) & S_{bd}&=\sin(4\pi^2 b\beta dL) & \mathbf{SI}_{bd}&=\mathrm{Si}(4\pi^2 b\beta dL)
\end{aligned}$$

$$\begin{aligned}
H_{ac}&=\,{}_2F_3\left(\frac{1}{2},\frac{1}{2};\frac{3}{2},\frac{3}{2},\frac{3}{2};-4\pi^4a^2\beta^2c^2L^2\right)\\
H_{ad}&=\,{}_2F_3\left(\frac{1}{2},\frac{1}{2};\frac{3}{2},\frac{3}{2},\frac{3}{2};-4\pi^4a^2\beta^2d^2L^2\right)\\
H_{bc}&=\,{}_2F_3\left(\frac{1}{2},\frac{1}{2};\frac{3}{2},\frac{3}{2},\frac{3}{2};-4\pi^4b^2\beta^2c^2L^2\right)\\
H_{bd}&=\,{}_2F_3\left(\frac{1}{2},\frac{1}{2};\frac{3}{2},\frac{3}{2},\frac{3}{2};-4\pi^4b^2\beta^2d^2L^2\right)
\end{aligned}$$

For the general case, we show as an example the results for the kernel integrals for $N_p = 0, 1, 5$:

$$\begin{aligned}
K_{\text{gen}}^{(n_s)}\Big|_{N_p=0}&=\int_c^d\int_a^b\left|\int_0^{L_s^{(n_s)}}e^{j4\pi^2 f_1' f_2' \beta_{2\text{eff}}^{(n_s)} z}\cdot p_0^{(n_s)}\,dz\right|^2 df_2' df_1'\\
&=p_0^2\cdot I_{00}^{(\text{gen})}\\
&=p_0^2\cdot\frac{1}{8\pi^4 ab\beta^2cd}\Big[4\pi^2 ab\beta cdL\,(-\mathbf{SI}_{ac}+\mathbf{SI}_{ad}+\mathbf{SI}_{bc}-\mathbf{SI}_{bd})\\
&\quad+8\pi^4 ab\beta^2cdL^2\,(2acH_{ac}-2adH_{ad}-2bcH_{bc}+2bdH_{bd})\\
&\quad-bdC_{ac}+adC_{bc}+bcC_{ad}-acC_{bd}+(a-b)(c-d)\Big]
\end{aligned}$$

$$
\begin{aligned}
K_{\text{gen}}^{(n_s)}\Big|_{N_p=1} &= \int_c^d \int_a^b \left| \int_0^{L_s^{(n_s)}} e^{j4\pi^2 f_1' f_2' \beta_{\text{2eff}}^{(n_s)} z} \cdot \left(p_0^{(n_s)} + p_1^{(n_s)} \cdot z \right) \mathrm{d}z \right|^2 \mathrm{d}f_2' \mathrm{d}f_1' \\
&= p_0^2 \cdot I_{00}^{(\text{gen})} + p_0 p_1 \cdot I_{01}^{(\text{gen})} + p_1^2 \cdot I_{11}^{(\text{gen})} \\
&= p_0^2 \cdot \frac{1}{8\pi^4 ab\beta^2 cd} \Bigg[4\pi^2 ab\beta cdL \left(-\mathbf{SI}_{ac} + \mathbf{SI}_{ad} + \mathbf{SI}_{bc} - \mathbf{SI}_{bd} \right) \\
&\quad + 8\pi^4 ab\beta^2 cdL^2 \left(2acH_{ac} - 2adH_{ad} - 2bcH_{bc} + 2bdH_{bd} \right) \\
&\quad - bdC_{ac} + adC_{bc} + bcC_{ad} - acC_{bd} + (a-b)(c-d) \Bigg] \\
&\quad + p_0 p_1 \cdot \Bigg[L^3 \left(2acH_{ac} - 2adH_{ad} - 2bcH_{bc} + 2bdH_{bd} \right) \\
&\quad - \frac{L^2}{2\pi^2 \beta} \left(\mathbf{SI}_{ac} - \mathbf{SI}_{ad} - \mathbf{SI}_{bc} + \mathbf{SI}_{bd} \right) \\
&\quad + \frac{L}{8\pi^4 ab\beta^2 cd} \left(bcC_{ad} - acC_{bd} - bdC_{ac} + adC_{bc} \right. \\
&\qquad \left. + ac - ad - bc + bd \right) \Bigg] \\
&\quad + p_1^2 \cdot \Bigg[\frac{L^4}{3} \left(2acH_{ac} - 2adH_{ad} - 2bcH_{bc} + 2bdH_{bd} \right) \\
&\quad + \frac{L^2}{144\pi^4 ab\beta^2 cd} \left(8bcC_{ad} - 8acC_{bd} - 8bdC_{ac} + 8adC_{bc} \right. \\
&\qquad \left. + 9ac - 9ad - 9bc + 9bd \right) \\
&\quad - \frac{2L^3}{9\pi^2 \beta} \left(\mathbf{SI}_{ac} - \mathbf{SI}_{ad} - \mathbf{SI}_{bc} + \mathbf{SI}_{bd} \right) \\
&\quad + \frac{L}{288\pi^6 a^2 b^2 \beta^3 c^2 d^2} \left(c^2 \left(b^2 S_{ad} - a^2 S_{bd} \right) + a^2 d^2 S_{bc} - b^2 d^2 S_{ac} \right) \\
&\quad + \frac{1}{1152\pi^8 a^3 b^3 \beta^4 c^3 d^3} \Bigg(-a^3 c^3 C_{bd} + a^3 d^3 C_{bc} + a^3 c^3 - a^3 d^3 \\
&\qquad + b^3 c^3 C_{ad} - b^3 d^3 C_{ac} - b^3 c^3 + b^3 d^3 \Bigg) \Bigg]
\end{aligned}
$$

$$
\begin{aligned}
K_{\text{gen}}^{(n_s)}\Big|_{N_p=5} &= \left| \int_d^c \int_a^b \int_0^{L_s^{(n_s)}} e^{j4\pi^2 f_1' f_2' \beta_{2\text{eff}}^{(n_s)} z} \cdot \left(\sum_{n=0}^{5} p_n^{(n_s)} \cdot z^n \right) dz\, df_2' df_1' \right|^2 \\
&= p_0^2 I_{00}^{(\text{gen})} + p_0 p_1 I_{01}^{(\text{gen})} + \cdots + p_5^2 I_{55}^{(\text{gen})} \\
&= p_0^2 \cdot \frac{1}{8\pi^4 ab\beta^2 cd} \Bigg[4\pi^2 ab\beta cdL \left(-\mathbf{SI}_{ac} + \mathbf{SI}_{ad} + \mathbf{SI}_{bc} - \mathbf{SI}_{bd} \right) \\
&\quad + 8\pi^4 ab\beta^2 cdL^2 \left(2acH_{ac} - 2adH_{ad} - 2bcH_{bc} + 2bdH_{bd} \right) \\
&\quad - bdC_{ac} + adC_{bc} + bcC_{ad} - acC_{bd} + (a-b)(c-d) \Bigg] \\
&\quad + p_0 p_1 \cdot \Bigg[L^3 \left(2acH_{ac} - 2adH_{ad} - 2bcH_{bc} + 2bdH_{bd} \right) \\
&\quad - \frac{L^2}{2\pi^2 \beta} \left(\mathbf{SI}_{ac} - \mathbf{SI}_{ad} - \mathbf{SI}_{bc} + \mathbf{SI}_{bd} \right) \\
&\quad + \frac{L}{8\pi^4 ab\beta^2 cd} \left(bcC_{ad} - acC_{bd} - bdC_{ac} + adC_{bc} \right. \\
&\qquad \left. + ac - ad - bc + bd \right) \Bigg] \\
&\quad + p_1^2 \cdot \Bigg[\frac{L^4}{3} \left(2acH_{ac} - 2adH_{ad} - 2bcH_{bc} + 2bdH_{bd} \right) \\
&\quad + \frac{L^2}{144\pi^4 ab\beta^2 cd} \left(8bcC_{ad} - 8acC_{bd} \right. \\
&\qquad \left. - 8bdC_{ac} + 8adC_{bc} + 9ac - 9ad - 9bc + 9bd \right) \\
&\quad - \frac{2L^3}{9\pi^2 \beta} \left(\mathbf{SI}_{ac} - \mathbf{SI}_{ad} - \mathbf{SI}_{bc} + \mathbf{SI}_{bd} \right) \\
&\quad + \frac{L}{288\pi^6 a^2 b^2 \beta^3 c^2 d^2} \left(c^2 \left(b^2 S_{ad} - a^2 S_{bd} \right) + a^2 d^2 S_{bc} - b^2 d^2 S_{ac} \right) \\
&\quad + \frac{1}{1152\pi^8 a^3 b^3 \beta^4 c^3 d^3} \Bigg(-a^3 c^3 C_{bd} + a^3 d^3 C_{bc} + a^3 c^3 - a^3 d^3 \\
&\qquad + b^3 c^3 C_{ad} - b^3 d^3 C_{ac} - b^3 c^3 + b^3 d^3 \Bigg) \Bigg] \\
&\quad + p_0 p_2 \cdot \Bigg[\frac{4L^4}{3} \left(acH_{ac} - adH_{ad} - bcH_{bc} + bdH_{bd} \right) \\
&\quad + \frac{1}{144\pi^8 \beta^4} \left(\frac{\sin^2(2\pi^2 a\beta dL)}{a^3 d^3} - \frac{\sin^2(2\pi^2 a\beta cL)}{a^3 c^3} \right.
\end{aligned}
$$

$$
\begin{aligned}
&\quad + \frac{\sin^2(2\pi^2 b\beta cL)}{b^3c^3} - \frac{\sin^2(2\pi^2 b\beta dL)}{b^3d^3}\Bigg) \\
&+ \frac{5L}{288\pi^6 a^2b^2\beta^3c^2d^2}\left(b^2c^2S_{ad} - b^2d^2S_{ac} + a^2d^2S_{bc} - a^2c^2S_{bd}\right) \\
&- \frac{11L^3}{18\pi^2\beta}\left(\mathbf{SI}_{ac} - \mathbf{SI}_{ad} - \mathbf{SI}_{bc} + \mathbf{SI}_{bd}\right) \\
&+ \frac{L^2}{72abcd\pi^4\beta^2}\Bigg[18(a-b)(c-d) \\
&\qquad - 11(bdC_{ac} - bcC_{ad} - adC_{bc} + acC_{bd})\Bigg]\Bigg] \\
&+ p_1p_2\cdot\Bigg[L^5\left(acH_{ac} - adH_{ad} - bcH_{bc} + bdH_{bd}\right) \\
&+ \frac{L^2}{128\pi^6 a^2b^2\beta^3c^2d^2}\left(c^2\left(b^2S_{ad} - a^2S_{bd}\right) + a^2d^2S_{bc} - b^2d^2S_{ac}\right) \\
&- \frac{3L^4}{8\pi^2\beta}\left(\mathbf{SI}_{ac} - \mathbf{SI}_{ad} - \mathbf{SI}_{bc} + \mathbf{SI}_{bd}\right) \\
&- \frac{L^3}{32\pi^4 ab\beta^2cd}\Bigg[3(bdC_{ac} - bcC_{ad} - adC_{bc} + acC_{bd}) \\
&\qquad -4(ac - ad - bc + bd)]\Bigg] \\
&+ p_2^2\cdot\Bigg[\frac{2L^6}{5}\left(acH_{ac} - adH_{ad} - bcH_{bc} + bdH_{bd}\right) \\
&+ \frac{1}{12800\pi^{12}a^5b^5\beta^6c^5d^5}\Bigg[-a^5c^5C_{bd} + a^5d^5C_{bc} + a^5c^5 - a^5d^5 \\
&\qquad + b^5c^5C_{ad} - b^5d^5C_{ac} - b^5c^5 + b^5d^5\Bigg] \\
&+ \frac{L}{3200\pi^{10}a^4b^4\beta^5c^4d^4}\left(c^4\left(b^4S_{ad} - a^4S_{bd}\right) + a^4d^4S_{bc} - b^4d^4S_{ac}\right) \\
&+ \frac{L^2}{1600\pi^8a^3b^3\beta^4c^3d^3}\left(c^3\left(a^3C_{bd} - b^3C_{ad}\right) - d^3\left(a^3C_{bc} - b^3C_{ac}\right)\right) \\
&+ \frac{7L^3}{1600\pi^6a^2b^2\beta^3c^2d^2}\left(c^2\left(b^2S_{ad} - a^2S_{bd}\right) + a^2d^2S_{bc} - b^2d^2S_{ac}\right) \\
&- \frac{17L^5}{100\pi^2\beta}\left(\mathbf{SI}_{ac} - \mathbf{SI}_{ad} - \mathbf{SI}_{bc} + \mathbf{SI}_{bd}\right) \\
&+ \frac{L^4}{400\pi^4ab\beta^2cd}\Bigg[17(bcC_{ad} - acC_{bd} - bdC_{ac} + adC_{bc})
\end{aligned}
$$

$$
\begin{aligned}
&\quad + 25(ac - ad - bc + bd)\Big]\Big] \\
&+ p_0 p_3 \cdot \Bigg[L^5 \left(acH_{ac} - adH_{ad} - bcH_{bc} + bdH_{bd}\right) \\
&\quad + \frac{3}{2048\pi^{10} a^4 b^4 \beta^5 c^4 d^4} \left(a^4 d^4 S_{ac} - a^4 c^4 S_{ad} + b^4 c^4 S_{bd} - b^4 d^4 S_{bc}\right) \\
&\quad + \frac{L}{1536\pi^8 a^3 b^3 \beta^4 c^3 d^3} \Bigg[7\left(a^3 d^3 C_{ac} - a^3 c^3 C_{ad} - b^3 d^3 C_{bc} + b^3 c^3 C_{bd}\right) \\
&\qquad + 16\left(a^3 c^3 - a^3 d^3 - b^3 c^3 + b^3 d^3\right)\Bigg] \\
&\quad + \frac{13 L^2}{768\pi^6 a^2 b^2 \beta^3 c^2 d^2} \left(b^2 c^2 S_{ad} - b^2 d^2 S_{ac} + a^2 d^2 S_{bc} - a^2 c^2 S_{bd}\right) \\
&\quad - \frac{25 L^4}{48\pi^2 \beta} \left(\mathbf{SI}_{ac} - \mathbf{SI}_{ad} - \mathbf{SI}_{bc} + \mathbf{SI}_{bd}\right) \\
&\quad + \frac{L^3}{192 abcd \pi^4 \beta^2} \Bigg[25(bdC_{ac} - bcC_{ad} - adC_{bc} + acC_{bd}) \\
&\qquad - 48(ac - ad - bc + bd)\Bigg]\Bigg] \\
&+ p_1 p_3 \cdot \Bigg[\frac{4 L^6}{5} \left(acH_{ac} - adH_{ad} - bcH_{bc} + bdH_{bd}\right) \\
&\quad - \frac{97 L^5}{300\pi^2 \beta} \left(\mathbf{SI}_{ac} - \mathbf{SI}_{ad} - \mathbf{SI}_{bc} + \mathbf{SI}_{bd}\right) \\
&\quad + \frac{L^4}{1200 abcd \pi^4 \beta^2} \Bigg[97(bcC_{ad} - acC_{bd} - bdC_{ac} + adC_{bc}) \\
&\qquad + 150(ac - ad - bc + bd)\Bigg] \\
&\quad - \frac{37 L^3}{4800 a^2 b^2 c^2 d^2 \pi^6 \beta^3} \left(c^2\left(a^2 S_{bd} - b^2 S_{ad}\right) + b^2 d^2 S_{ac} - a^2 d^2 S_{bc}\right) \\
&\quad + \frac{L^2}{9600 a^3 b^3 c^3 d^3 \pi^8 \beta^4} \Bigg[7\left(b^3 c^3 C_{ad} - a^3 c^3 C_{bd} - b^3 d^3 C_{ac} + a^3 d^3 C_{bc}\right) \\
&\qquad + 25\left(b^3 c^3 - a^3 c^3 + a^3 d^3 - b^3 d^3\right)\Bigg] \\
&\quad + \frac{3L}{3200 a^4 b^4 c^4 d^4 \pi^{10} \beta^5} \left(c^4\left(a^4 S_{bd} - b^4 S_{ad}\right) + b^4 d^4 S_{ac} - a^4 d^4 S_{bc}\right) \\
&\quad + \frac{3}{12800 a^5 b^5 c^5 d^5 \pi^{12} \beta^6} \Bigg[5\left(b^5 c^5 - a^5 c^5 + a^5 d^5 - b^5 d^5\right)
\end{aligned}
$$

$$+ 3\left(a^5c^5C_{bd} - b^5c^5C_{ad} + b^5d^5C_{ac} - a^5d^5C_{bc}\right)\Bigg]\Bigg]$$

$$+ p_2p_3 \cdot \Bigg[\frac{2L^7}{3}\left(acH_{ac} - adH_{ad} - bcH_{bc} + bdH_{bd}\right)$$

$$+ \frac{L^3}{576\pi^8a^3b^3\beta^4c^3d^3}\Bigg[a^3c^3C_{bd} - a^3d^3C_{bc} - a^3c^3 + a^3d^3$$

$$- b^3c^3C_{ad} + b^3d^3C_{ac} + b^3c^3 - b^3d^3\Bigg]$$

$$+ \frac{5L^4}{576\pi^6a^2b^2\beta^3c^2d^2}\left(c^2\left(b^2S_{ad} - a^2S_{bd}\right) + a^2d^2S_{bc} - b^2d^2S_{ac}\right)$$

$$- \frac{11L^6}{36\pi^2\beta}\left(\mathbf{SI}_{ac} - \mathbf{SI}_{ad} - \mathbf{SI}_{bc} + \mathbf{SI}_{bd}\right)$$

$$+ \frac{L^5}{144\pi^4ab\beta^2cd}\Bigg[11(bcC_{ad} - acC_{bd} - bdC_{ac} + adC_{bc})$$

$$+ 18(ac - ad - bc + bd)\Bigg]\Bigg]$$

$$+ p_3^2 \cdot \Bigg[\frac{2L^8}{7}\left(acH_{ac} - adH_{ad} - bcH_{bc} + bdH_{bd}\right)$$

$$- \frac{83L^7}{588\pi^2\beta}\left(\mathbf{SI}_{ac} - \mathbf{SI}_{ad} - \mathbf{SI}_{bc} + \mathbf{SI}_{bd}\right)$$

$$+ \frac{L^6}{2352abcd\pi^4\beta^2}\Bigg[83(bcC_{ad} - acC_{bd} - bdC_{ac} + adC_{bc})$$

$$+ 147(ac - ad - bc + bd)\Bigg]$$

$$- \frac{41L^5}{9408a^2b^2c^2d^2\pi^6\beta^3}\left(c^2\left(a^2S_{bd} - b^2S_{ad}\right) + b^2d^2S_{ac} - a^2d^2S_{bc}\right)$$

$$+ \frac{L^4}{37632a^3b^3c^3d^3\pi^8\beta^4}\Bigg[40\left(b^3c^3C_{ad} - a^3c^3C_{bd} - b^3d^3C_{ac} + a^3d^3C_{bc}\right)$$

$$+ 49\left(b^3c^3 - a^3c^3 + a^3d^3 - b^3d^3\right)\Bigg]$$

$$+ \frac{3L^3}{12544a^4b^4c^4d^4\pi^{10}\beta^5}\left(c^4\left(a^4S_{bd} - b^4S_{ad}\right) + b^4d^4S_{ac} - a^4d^4S_{bc}\right)$$

$$+ \frac{9L^2}{50176a^5b^5c^5d^5\pi^{12}\beta^6}\left(c^5\left(a^5C_{bd} - b^5C_{ad}\right) + b^5d^5C_{ac} - a^5d^5C_{bc}\right)$$

$$+ \frac{9L}{100352a^6b^6c^6d^6\pi^{14}\beta^7}\left(c^6\left(b^6S_{ad} - a^6S_{bd}\right) + a^6d^6S_{bc} - b^6d^6S_{ac}\right)$$

$$
\begin{aligned}
&- \frac{9}{401408 a^7 b^7 c^7 d^7 \pi^{16} \beta^8} \Bigg[7 \left(b^7 c^7 - a^7 c^7 + a^7 d^7 - b^7 d^7 \right) \\
&\qquad + 9 \left(a^7 c^7 C_{bd} - b^7 c^7 C_{ad} + b^7 d^7 C_{ac} - a^7 d^7 C_{bc} \right) \Bigg] \Bigg] \\
&+ p_0 p_4 \cdot \Bigg[\frac{4 L^6}{5} \left(ac H_{ac} - ad H_{ad} - bc H_{bc} + bd H_{bd} \right) \\
&\quad - \frac{137 L^5}{300 \pi^2 \beta} \left(\mathbf{SI}_{ac} - \mathbf{SI}_{ad} - \mathbf{SI}_{bc} + \mathbf{SI}_{bd} \right) \\
&\quad + \frac{L^4}{1200 abcd \pi^4 \beta^2} \Bigg[300 (a-b)(c-d) \\
&\qquad - 137 (bd C_{ac} - bc C_{ad} - ad C_{bc} + ac C_{bd}) \Bigg] \\
&\quad + \frac{77 L^3}{4800 a^2 b^2 c^2 d^2 \pi^6 \beta^3} \left(b^2 c^2 S_{ad} - b^2 d^2 S_{ac} + a^2 d^2 S_{bc} - a^2 c^2 S_{bd} \right) \\
&\quad + \frac{L^2}{9600 a^3 b^3 c^3 d^3 \pi^8 \beta^4} \Bigg[200 \left(a^3 d^3 - a^3 c^3 - b^3 c^3 + b^3 d^3 \right) \\
&\qquad + 47 \left(b^3 d^3 C_{ac} - b^3 c^3 C_{ad} - a^3 d^3 C_{bc} + a^3 c^3 C_{bd} \right) \Bigg] \\
&\quad + \frac{27 L}{12800 a^4 b^4 c^4 d^4 \pi^{10} \beta^5} \left(b^4 d^4 S_{ac} - b^4 c^4 S_{ad} + a^4 c^4 S_{bd} - a^4 d^4 S_{bc} \right) \\
&\quad + \frac{3}{1600 a^5 b^5 c^5 d^5 \pi^{12} \beta^6} \Bigg[a^5 c^5 \sin^2 \left(2bdL\pi^2\beta \right) - a^5 d^5 \sin^2 \left(2bcL\pi^2\beta \right) \\
&\qquad + b^5 d^5 \sin^2 \left(2acL\pi^2\beta \right) - b^5 c^5 \sin^2 \left(2adL\pi^2\beta \right) \Bigg] \Bigg] \\
&+ p_1 p_4 \cdot \Bigg[\frac{2 L^7}{3} \left(ac H_{ac} - ad H_{ad} - bc H_{bc} + bd H_{bd} \right) \\
&\quad + \frac{3 L^2}{2048 \pi^{10} a^4 b^4 \beta^5 c^4 d^4} \left(c^4 \left(a^4 S_{bd} - b^4 S_{ad} \right) - a^4 d^4 S_{bc} + b^4 d^4 S_{ac} \right) \\
&\quad + \frac{L^3}{4608 \pi^8 a^3 b^3 \beta^4 c^3 d^3} \Bigg[5 \left(a^3 c^3 C_{bd} - a^3 d^3 C_{bc} - b^3 c^3 C_{ad} + b^3 d^3 C_{ac} \right) \\
&\qquad + 32 \left(b^3 c^3 - a^3 c^3 + a^3 d^3 - b^3 d^3 \right) \Bigg] \\
&\quad - \frac{17 L^4}{2304 \pi^6 a^2 b^2 \beta^3 c^2 d^2} \left(c^2 \left(a^2 S_{bd} - b^2 S_{ad} \right) - a^2 d^2 S_{bc} + b^2 d^2 S_{ac} \right) \\
&\quad - \frac{41 L^6}{144 \pi^2 \beta} \left(\mathbf{SI}_{ac} - \mathbf{SI}_{ad} - \mathbf{SI}_{bc} + \mathbf{SI}_{bd} \right)
\end{aligned}
$$

$$
\begin{aligned}
&+\frac{L^5}{576\pi^4 ab\beta^2 cd}\Bigg[41(bcC_{ad}-acC_{bd}-bdC_{ac}+adC_{bc})\\
&\qquad+72(ac-ad-bc+bd)\Bigg]\Bigg]\\
&+p_2p_4\cdot\Bigg[\frac{4L^8}{7}\left(acH_{ac}-adH_{ad}-bcH_{bc}+bdH_{bd}\right)\\
&-\frac{325L^7}{1176\pi^2\beta}\left(\mathbf{SI}_{ac}-\mathbf{SI}_{ad}-\mathbf{SI}_{bc}+\mathbf{SI}_{bd}\right)\\
&+\frac{L^6}{4704abcd\pi^4\beta^2}\Bigg[325(bcC_{ad}-acC_{bd}-bdC_{ac}+adC_{bc})\\
&\qquad+588(ac-ad-bc+bd)\Bigg]\\
&-\frac{157L^5}{18816a^2b^2c^2d^2\pi^6\beta^3}\left(c^2\left(a^2S_{bd}-b^2S_{ad}\right)+b^2d^2S_{ac}-a^2d^2S_{bc}\right)\\
&+\frac{L^4}{37632a^3b^3c^3d^3\pi^8\beta^4}\Bigg[73\left(b^3c^3C_{ad}-a^3c^3C_{bd}-b^3d^3C_{ac}+a^3d^3C_{bc}\right)\\
&\qquad+196\left(b^3c^3-a^3c^3+a^3d^3-b^3d^3\right)\Bigg]\\
&+\frac{17L^3}{50176a^4b^4c^4d^4\pi^{10}\beta^5}\left(c^4\left(a^4S_{bd}-b^4S_{ad}\right)+b^4d^4S_{ac}-a^4d^4S_{bc}\right)\\
&+\frac{3L^2}{6272a^5b^5c^5d^5\pi^{12}\beta^6}\left(c^5\left(b^5C_{ad}-a^5C_{bd}\right)-b^5d^5C_{ac}+a^5d^5C_{bc}\right)\\
&+\frac{3L}{12544a^6b^6c^6d^6\pi^{14}\beta^7}\left(c^6\left(a^6S_{bd}-b^6S_{ad}\right)+b^6d^6S_{ac}-a^6d^6S_{bc}\right)\\
&+\frac{3}{50176a^7b^7c^7d^7\pi^{16}\beta^8}\Bigg[7\left(b^7c^7-a^7c^7+a^7d^7-b^7d^7\right)\\
&\qquad+3\left(a^7c^7C_{bd}-b^7c^7C_{ad}+b^7d^7C_{ac}-a^7d^7C_{bc}\right)\Bigg]\Bigg]\\
&+p_3p_4\cdot\Bigg[\frac{L^9}{2}\left(acH_{ac}-adH_{ad}-bcH_{bc}+bdH_{bd}\right)\\
&+\frac{3L^4}{4096\pi^{10}a^4b^4\beta^5c^4d^4}\left(c^4\left(a^4S_{bd}-b^4S_{ad}\right)-a^4d^4S_{bc}+b^4d^4S_{ac}\right)\\
&+\frac{L^5}{3072\pi^8a^3b^3\beta^4c^3d^3}\Bigg[7\left(a^3c^3C_{bd}-a^3d^3C_{bc}-b^3c^3C_{ad}+b^3d^3C_{ac}\right)\\
&\qquad+16\left(b^3c^3-a^3c^3+a^3d^3-b^3d^3\right)\Bigg]
\end{aligned}
$$

$$
\begin{aligned}
&- \frac{13L^6}{1536\pi^6 a^2b^2\beta^3c^2d^2}\left(c^2\left(a^2S_{bd}-b^2S_{ad}\right)-a^2d^2S_{bc}+b^2d^2S_{ac}\right)\\
&- \frac{25L^8}{96\pi^2\beta}\left(\mathbf{SI}_{ac}-\mathbf{SI}_{ad}-\mathbf{SI}_{bc}+\mathbf{SI}_{bd}\right)\\
&+ \frac{L^7}{384\pi^4 ab\beta^2cd}\Bigg[25(bcC_{ad}-acC_{bd}-bdC_{ac}+adC_{bc})\\
&\qquad + 48(ac-ad-bc+bd)\Bigg]\Bigg]\\
+ p_4^2\cdot\Bigg[&\frac{2L^{10}}{9}\left(acH_{ac}-adH_{ad}-bcH_{bc}+bdH_{bd}\right)\\
&- \frac{79L^9}{648\pi^2\beta}\left(\mathbf{SI}_{ac}-\mathbf{SI}_{ad}-\mathbf{SI}_{bc}+\mathbf{SI}_{bd}\right)\\
&+ \frac{L^8}{2592abcd\pi^4\beta^2}\Bigg[79(bcC_{ad}-acC_{bd}-bdC_{ac}+adC_{bc})\\
&\qquad + 162(ac-ad-bc+bd)\Bigg]\\
&- \frac{43L^7}{10368a^2b^2c^2d^2\pi^6\beta^3}\left(c^2\left(a^2S_{bd}-b^2S_{ad}\right)+b^2d^2S_{ac}-a^2d^2S_{bc}\right)\\
&+ \frac{L^6}{20736a^3b^3c^3d^3\pi^8\beta^4}\Bigg[25\left(b^3c^3C_{ad}-a^3c^3C_{bd}-b^3d^3C_{ac}+a^3d^3C_{bc}\right)\\
&\qquad + 72\left(b^3c^3-a^3c^3+a^3d^3-b^3d^3\right)\Bigg]\\
&+ \frac{13L^5}{27648a^4b^4c^4d^4\pi^{10}\beta^5}\left(c^4\left(a^4S_{bd}-b^4S_{ad}\right)+b^4d^4S_{ac}-a^4d^4S_{bc}\right)\\
&+ \frac{L^4}{6912a^5b^5c^5d^5\pi^{12}\beta^6}\left(c^5\left(b^5C_{ad}-a^5C_{bd}\right)-b^5d^5C_{ac}+a^5d^5C_{bc}\right)\\
&+ \frac{L^3}{6912a^6b^6c^6d^6\pi^{14}\beta^7}\left(c^6\left(a^6S_{bd}-b^6S_{ad}\right)+b^6d^6S_{ac}-a^6d^6S_{bc}\right)\\
&+ \frac{L^2}{9216a^7b^7c^7d^7\pi^{16}\beta^8}\left(c^7\left(a^7C_{bd}-b^7C_{ad}\right)+b^7d^7C_{ac}-a^7d^7C_{bc}\right)\\
&+ \frac{L}{18432a^8b^8c^8d^8\pi^{18}\beta^9}\left(c^8\left(b^8S_{ad}-a^8S_{bd}\right)+a^8d^8S_{bc}-b^8d^8S_{ac}\right)\\
&+ \frac{1}{73728a^9b^9c^9d^9\pi^{20}\beta^{10}}\Bigg[9\left(a^9c^9-b^9c^9-a^9d^9+b^9d^9\right)\\
&\qquad + 9\left(b^9c^9C_{ad}-a^9c^9C_{bd}-b^9d^9C_{ac}+a^9d^9C_{bc}\right)\Bigg]\Bigg]
\end{aligned}
$$

$$
\begin{aligned}
&+ p_0 p_5 \cdot \Bigg[\frac{2L^7}{3} \left(acH_{ac} - adH_{ad} - bcH_{bc} + bdH_{bd} \right) \\
&\quad - \frac{49L^6}{120\pi^2\beta} \left(\mathbf{SI}_{ac} - \mathbf{SI}_{ad} - \mathbf{SI}_{bc} + \mathbf{SI}_{bd} \right) \\
&\quad + \frac{L^5}{480abcd\pi^4\beta^2} \Bigg[120(a-b)(c-d) \\
&\qquad\qquad - 49(bdC_{ac} - bcC_{ad} - adC_{bc} + acC_{bd}) \Bigg] \\
&\quad + \frac{29L^4}{1920a^2b^2c^2d^2\pi^6\beta^3} \left(b^2c^2S_{ad} - b^2d^2S_{ac} + a^2d^2S_{bc} - a^2c^2S_{bd} \right) \\
&\quad + \frac{L^3}{3840a^3b^3c^3d^3\pi^8\beta^4} \Bigg[19 \left(b^3d^3C_{ac} - b^3c^3C_{ad} - a^3d^3C_{bc} + a^3c^3C_{bd} \right) \\
&\qquad\qquad + 100 \left(a^3d^3 - a^3c^3 - b^3c^3 + b^3d^3 \right) \Bigg] \\
&\quad + \frac{37L^2}{15360a^4b^4c^4d^4\pi^{10}\beta^5} \left(b^4d^4S_{ac} - b^4c^4S_{ad} + a^4c^4S_{bd} - a^4d^4S_{bc} \right) \\
&\quad + \frac{L}{7680a^5b^5c^5d^5\pi^{12}\beta^6} \Bigg[11 \left(b^5d^5C_{ac} - b^5c^5C_{ad} - a^5d^5C_{bc} + a^5c^5C_{bd} \right) \\
&\qquad\qquad + 36 \left(a^5d^5 - a^5c^5 - b^5c^5 + b^5d^5 \right) \Bigg] \\
&\quad + \frac{5}{61440a^6b^6c^6d^6\pi^{14}\beta^7} \left(b^6c^6S_{ad} - b^6d^6S_{ac} + a^6d^6S_{bc} - a^6c^6S_{bd} \right) \Bigg] \\
&+ p_1 p_5 \cdot \Bigg[\frac{4L^8}{7} \left(acH_{ac} - adH_{ad} - bcH_{bc} + bdH_{bd} \right) \\
&\quad - \frac{1499L^7}{5880\pi^2\beta} \left(\mathbf{SI}_{ac} - \mathbf{SI}_{ad} - \mathbf{SI}_{bc} + \mathbf{SI}_{bd} \right) \\
&\quad + \frac{L^6}{23520abcd\pi^4\beta^2} \Bigg[1499(bcC_{ad} - acC_{bd} - bdC_{ac} + adC_{bc}) \\
&\qquad\qquad + 2940(ac - ad - bc + bd) \Bigg] \\
&\quad - \frac{659L^5}{94080a^2b^2c^2d^2\pi^6\beta^3} \left(c^2 \left(a^2S_{bd} - b^2S_{ad} \right) + b^2d^2S_{ac} - a^2d^2S_{bc} \right) \\
&\quad + \frac{L^4}{188160a^3b^3c^3d^3\pi^8\beta^4} \Bigg[239 \left(b^3c^3C_{ad} - a^3c^3C_{bd} - b^3d^3C_{ac} + a^3d^3C_{bc} \right) \\
&\qquad\qquad + 2450 \left(b^3c^3 - a^3c^3 + a^3d^3 - b^3d^3 \right) \Bigg]
\end{aligned}
$$

$$
\begin{aligned}
&+\frac{449L^3}{250880a^4b^4c^4d^4\pi^{10}\beta^5}\left(c^4\left(a^4S_{bd}-b^4S_{ad}\right)+b^4d^4S_{ac}-a^4d^4S_{bc}\right)\\
&+\frac{3L^2}{125440a^5b^5c^5d^5\pi^{12}\beta^6}\Bigg[1\left(a^5c^5C_{bd}-b^5c^5C_{ad}+b^5d^5C_{ac}-a^5d^5C_{bc}\right)\\
&\qquad\qquad+49\left(a^5c^5-b^5c^5-a^5d^5+b^5d^5\right)\Bigg]\\
&-\frac{15L}{250880a^6b^6c^6d^6\pi^{14}\beta^7}\left(c^6\left(a^6S_{bd}-b^6S_{ad}\right)+b^6d^6S_{ac}-a^6d^6S_{bc}\right)\\
&-\frac{15}{1003520a^7b^7c^7d^7\pi^{16}\beta^8}\Bigg[7\left(b^7c^7-a^7c^7+a^7d^7-b^7d^7\right)\\
&\qquad\qquad+15\left(a^7c^7C_{bd}-b^7c^7C_{ad}+b^7d^7C_{ac}-a^7d^7C_{bc}\right)\Bigg]\Bigg]\\
&+p_2p_5\cdot\Bigg[\frac{L^9}{2}\left(acH_{ac}-adH_{ad}-bcH_{bc}+bdH_{bd}\right)\\
&-\frac{121L^8}{480\pi^2\beta}\left(\mathbf{SI}_{ac}-\mathbf{SI}_{ad}-\mathbf{SI}_{bc}+\mathbf{SI}_{bd}\right)\\
&+\frac{L^7}{1920abcd\pi^4\beta^2}\Bigg[121(bcC_{ad}-acC_{bd}-bdC_{ac}+adC_{bc})\\
&\qquad\qquad+240(ac-ad-bc+bd)\Bigg]\\
&-\frac{61L^6}{7680a^2b^2c^2d^2\pi^6\beta^3}\left(c^2\left(a^2S_{bd}-b^2S_{ad}\right)+b^2d^2S_{ac}-a^2d^2S_{bc}\right)\\
&+\frac{L^5}{15360a^3b^3c^3d^3\pi^8\beta^4}\Bigg[31\left(b^3c^3C_{ad}-a^3c^3C_{bd}-b^3d^3C_{ac}+a^3d^3C_{bc}\right)\\
&\qquad\qquad+160\left(b^3c^3-a^3c^3+a^3d^3-b^3d^3\right)\Bigg]\\
&+\frac{11L^4}{20480a^4b^4c^4d^4\pi^{10}\beta^5}\left(c^4\left(a^4S_{bd}-b^4S_{ad}\right)+b^4d^4S_{ac}-a^4d^4S_{bc}\right)\\
&+\frac{L^3}{1280a^5b^5c^5d^5\pi^{12}\beta^6}\Bigg[a^5c^5-b^5c^5-a^5d^5+b^5d^5\\
&\qquad\qquad+b^5c^5C_{ad}-a^5c^5C_{bd}-b^5d^5C_{ac}+a^5d^5C_{bc}\Bigg]\Bigg]\\
&+p_3p_5\cdot\Bigg[\frac{4L^{10}}{9}\left(acH_{ac}-adH_{ad}-bcH_{bc}+bdH_{bd}\right)\\
&-\frac{781L^9}{3240\pi^2\beta}\left(\mathbf{SI}_{ac}-\mathbf{SI}_{ad}-\mathbf{SI}_{bc}+\mathbf{SI}_{bd}\right)
\end{aligned}
$$

$$
\begin{aligned}
&+\frac{L^8}{12960abcd\pi^4\beta^2}\Bigg[781(bcC_{ad}-acC_{bd}-bdC_{ac}+adC_{bc})\\
&\qquad\qquad+1620(ac-ad-bc+bd)\Bigg]\\
&-\frac{421L^7}{51840a^2b^2c^2d^2\pi^6\beta^3}\left(c^2\left(a^2S_{bd}-b^2S_{ad}\right)+b^2d^2S_{ac}-a^2d^2S_{bc}\right)\\
&+\frac{L^6}{103680a^3b^3c^3d^3\pi^8\beta^4}\Bigg[241\left(b^3c^3C_{ad}-a^3c^3C_{bd}-b^3d^3C_{ac}+a^3d^3C_{bc}\right)\\
&\qquad\qquad+990\left(b^3c^3-a^3c^3+a^3d^3-b^3d^3\right)\Bigg]\\
&+\frac{121L^5}{138240a^4b^4c^4d^4\pi^{10}\beta^5}\left(c^4\left(a^4S_{bd}-b^4S_{ad}\right)+b^4d^4S_{ac}-a^4d^4S_{bc}\right)\\
&+\frac{L^4}{138240a^5b^5c^5d^5\pi^{12}\beta^6}\Bigg[31\left(b^5c^5C_{ad}-a^5c^5C_{bd}-b^5d^5C_{ac}+a^5d^5C_{bc}\right)\\
&\qquad\qquad+81\left(a^5c^5-b^5c^5-a^5d^5+b^5d^5\right)\Bigg]\\
&+\frac{5L^3}{13824a^6b^6c^6d^6\pi^{14}\beta^7}\left(c^6\left(b^6S_{ad}-a^6S_{bd}\right)-b^6d^6S_{ac}+a^6d^6S_{bc}\right)\\
&+\frac{5L^2}{18432a^7b^7c^7d^7\pi^{16}\beta^8}\left(c^7\left(C_{ad}a^7-C_{bd}b^7\right)-d^7\left(C_{ac}b^7-C_{bc}a^7\right)\right)\\
&+\frac{5L}{36864a^8b^8c^8d^8\pi^{18}\beta^9}\left(c^8\left(a^8S_{bd}-b^8S_{ad}\right)+b^8d^8S_{ac}-a^8d^8S_{bc}\right)\\
&+\frac{5}{147456a^9b^9c^9d^9\pi^{20}\beta^{10}}\Bigg[9\left(b^9c^9-a^9c^9+a^9d^9-b^9d^9\right)\\
&\qquad\qquad+5\left(a^9c^9C_{bd}-b^9c^9C_{ad}+b^9d^9C_{ac}-a^9d^9C_{bc}\right)\Bigg]\Bigg]\\
&+p_4p_5\cdot\Bigg[\frac{2L^{11}}{5}\left(acH_{ac}-adH_{ad}-bcH_{bc}+bdH_{bd}\right)\\
&-\frac{137L^{10}}{600\pi^2\beta}\left(\mathbf{SI}_{ac}-\mathbf{SI}_{ad}-\mathbf{SI}_{bc}+\mathbf{SI}_{bd}\right)\\
&+\frac{L^9}{2400abcd\pi^4\beta^2}\Bigg[137(bcC_{ad}-acC_{bd}-bdC_{ac}+adC_{bc})\\
&\qquad\qquad+300(ac-ad-bc+bd)\Bigg]\\
&-\frac{77L^8}{9600a^2b^2c^2d^2\pi^6\beta^3}\left(c^2\left(a^2S_{bd}-b^2S_{ad}\right)+b^2d^2S_{ac}-a^2d^2S_{bc}\right)
\end{aligned}
$$

$$
\begin{aligned}
&+\frac{L^7}{19200a^3b^3c^3d^3\pi^8\beta^4}\Bigg[47\left(b^3c^3C_{ad}-a^3c^3C_{bd}-b^3d^3C_{ac}+a^3d^3C_{bc}\right)\\
&\qquad\qquad+200\left(b^3c^3-a^3c^3+a^3d^3-b^3d^3\right)\Bigg]\\
&+\frac{27L^6}{25600a^4b^4c^4d^4\pi^{10}\beta^5}\left(c^4\left(a^4S_{bd}-b^4S_{ad}\right)+b^4d^4S_{ac}-a^4d^4S_{bc}\right)\\
&-\frac{3L^5}{6400a^5b^5c^5d^5\pi^{12}\beta^6}\Bigg[b^5c^5-a^5c^5+a^5d^5-b^5d^5\\
&\qquad\qquad+a^5c^5C_{bd}-b^5c^5C_{ad}+b^5d^5C_{ac}-a^5d^5C_{bc}\Bigg]\Bigg]\\
&+p_5^2\cdot\Bigg[\frac{2L^{12}}{11}\left(acH_{ac}-adH_{ad}-bcH_{bc}+bdH_{bd}\right)\\
&-\frac{1567L^{11}}{14520\pi^2\beta}\left(\mathbf{SI}_{ac}-\mathbf{SI}_{ad}-\mathbf{SI}_{bc}+\mathbf{SI}_{bd}\right)\\
&+\frac{L^{10}}{58080abcd\pi^4\beta^2}\Bigg[1567(bcC_{ad}-acC_{bd}-bdC_{ac}+adC_{bc})\\
&\qquad\qquad+3630(ac-ad-bc+bd)\Bigg]\\
&-\frac{907L^9}{232320a^2b^2c^2d^2\pi^6\beta^3}\left(c^2\left(a^2S_{bd}-b^2S_{ad}\right)+b^2d^2S_{ac}-a^2d^2S_{bc}\right)\\
&+\frac{L^8}{464640a^3b^3c^3d^3\pi^8\beta^4}\Bigg[577\left(b^3c^3C_{ad}-a^3c^3C_{bd}-b^3d^3C_{ac}+a^3d^3C_{bc}\right)\\
&\qquad\qquad+3025\left(b^3c^3-a^3c^3+a^3d^3-b^3d^3\right)\Bigg]\\
&+\frac{357L^7}{619520a^4b^4c^4d^4\pi^{10}\beta^5}\left(c^4\left(a^4S_{bd}-b^4S_{ad}\right)+b^4d^4S_{ac}-a^4d^4S_{bc}\right)\\
&+\frac{L^6}{309760a^5b^5c^5d^5\pi^{12}\beta^6}\Bigg[96\left(b^5c^5C_{ad}-a^5c^5C_{bd}-b^5d^5C_{ac}+a^5d^5C_{bc}\right)\\
&\qquad\qquad+121\left(a^5c^5-b^5c^5-a^5d^5+b^5d^5\right)\Bigg]\\
&-\frac{15L^5}{123904a^6b^6c^6d^6\pi^{14}\beta^7}\left(c^6\left(a^6S_{bd}-b^6S_{ad}\right)+b^6d^6S_{ac}-a^6d^6S_{bc}\right)\\
&-\frac{75L^4}{495616a^7b^7c^7d^7\pi^{16}\beta^8}\left(c^7\left(a^7C_{bd}-b^7C_{ad}\right)+b^7d^7C_{ac}-a^7d^7C_{bc}\right)\\
&+\frac{75L^3}{495616a^8b^8c^8d^8\pi^{18}\beta^9}\left(c^8\left(b^8S_{ad}-a^8S_{bd}\right)+a^8d^8S_{bc}-b^8d^8S_{ac}\right)
\end{aligned}
$$

$$
\begin{aligned}
&+ \frac{225L^2}{1982464a^9b^9c^9d^9\pi^{20}\beta^{10}} \left(c^9\left(a^9C_{bd} - b^9C_{ad}\right) + b^9d^9C_{ac} - a^9d^9C_{bc}\right) \\
&- \frac{225L}{3964928a^{10}b^{10}c^{10}d^{10}\pi^{22}\beta^{11}} \Bigg(c^{10}\left(a^{10}S_{bd} - b^{10}S_{ad}\right) \\
&\qquad\qquad + b^{10}d^{10}S_{ac} - a^{10}d^{10}S_{bc} \Bigg) \\
&- \frac{225}{15859712a^{11}b^{11}c^{11}d^{11}\pi^{24}\beta^{12}} \Bigg[11\left(b^{11}c^{11} - a^{11}c^{11} + a^{11}d^{11} - b^{11}d^{11}\right) \\
&\qquad\qquad + 11\left(a^{11}c^{11}C_{bd} - b^{11}c^{11}C_{ad}\right) \\
&\qquad\qquad + 11\left(b^{11}d^{11}C_{ac} - a^{11}d^{11}C_{bc}\right) \Bigg] \Bigg]
\end{aligned}
$$

Note that to simplify the notation, we replace the term $p_n^{(n_s)}$ with the shorthand p_n for any generic index $n = 0, 1, 2, \ldots$. For example, $p_0^{(n_s)}$ is written as p_0, and $p_1^{(n_s)}$ is written as p_1.

For any value of N_p, what we need to do is simply multiply these analytical solutions by the corresponding polynomial coefficients and then sum them up according to Eq. (43). We can notice that the characteristic of reusability brought by the summation structure still holds here. Also we still present the solution as a weighted sum of the fundamental integral terms and use same structure as Section 4.1 in our C/MEX code.

As the degree increases, the length of the analytical solution for the newly introduced $I_{nm}^{(\mathrm{gen})}$ grows a lot, resulting in a final result too large for representation. So here we present the result only up to the polynomial degree $N_p = 5$.

4.3 Solution Verification

4.3.1 Single-Mode Fiber Ultra-Wideband Long-Haul scenario

To provide a rigorous and comprehensive validation of our derived general analytical solution of the highest degree we can currently reach ($N_p = 7$), we designed a detailed test plan that focuses on a Single-Mode Fiber (SMF) Ultra-Wideband (UWB) Long-Haul System (see Figure 9). This test aims to prove the solutions' accuracy by in a high dispersion and a high symbol rate system. The simulations are conducted over a **100km** segment of SMF, incorporating its full frequency-dependent characteristics. The WDM signal is structured with **50 channels per band**. Each channel operates at a **100GBaud symbol rate** and the signals are separated by a consistent **118.75GHz channel spacing**. To con-

trol inter-symbol interference, the signal pulses are shaped using a SRRC filter with a low **roll-off factor of 0.1**.

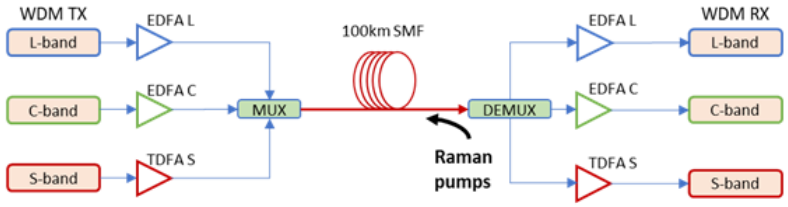

Figure 9: SMF UWB Long-Haul System schematic.

1. **Channel Selection ($\mathbf{n_{CUT}}$)**: To ensure full spectral coverage, we select three distinct n_{CUT}, that is $\mathbf{n_{CUT} = 25}$ from the L-band, $\mathbf{n_{CUT} = 75}$ from the C-band, and $\mathbf{n_{CUT} = 125}$ from the S-band.

2. **Three Spatial Power Profile (SPP) Scenarios** : Each n_{CUT} will be tested under three different SPP cases:

   - **Case 1: C+L+S: ISRS off, no Raman**. This scenario provides the simplest, non-tilted SPP profile, confirming the analytical solution's accuracy under baseline conditions.

   - **Case 2: C+L+S: ISRS on, no Raman**. This tests the model's ability to handle the inevitable spectral tilt caused by ISRS in UWB Long-Haul systems.

   - **Case 3: C+L+S: ISRS on + 3 Pumps**. This simulates a fully operational UWB Long-Haul system with three active Raman pumps and the ISRS-induced spectral tilt, verifying the model's precision in handling the highly dynamic and complex power profile.

     The exact SPPs of three chosen channels ($n_{\text{CUT}} = 25, 75, 125$) under three scenarios above is shown in Figure 10. In test we will use the SPPs in the form of polynomial representation, and use that of Np=7 for our result and that of Np=9 for numerical integration. The accuracy of polynomial representation against exact numerical value at $N_p = 7$ and $N_p = 9$ has already been shown in Figure 6. Further comprehensive validation can be found in the [16].

For each n_{CUT} and each SPP case, we separately isolate and verify the prediction accuracy of the core Non-Linear Interference (NLI) components. The Self-Channel Interference (SCI) is validated using n_{CUT} itself. We choose to validate Cross-Channel Interference (XCI) and Multi-Channel Interference (MCI) using only the nearest neighboring channel because they have largest non-linear contribution to n_{CUT}. Specifically, XCI is validated by considering the contribution from the channel on the horizontally right (i.e., $k_{\text{ch}} =$

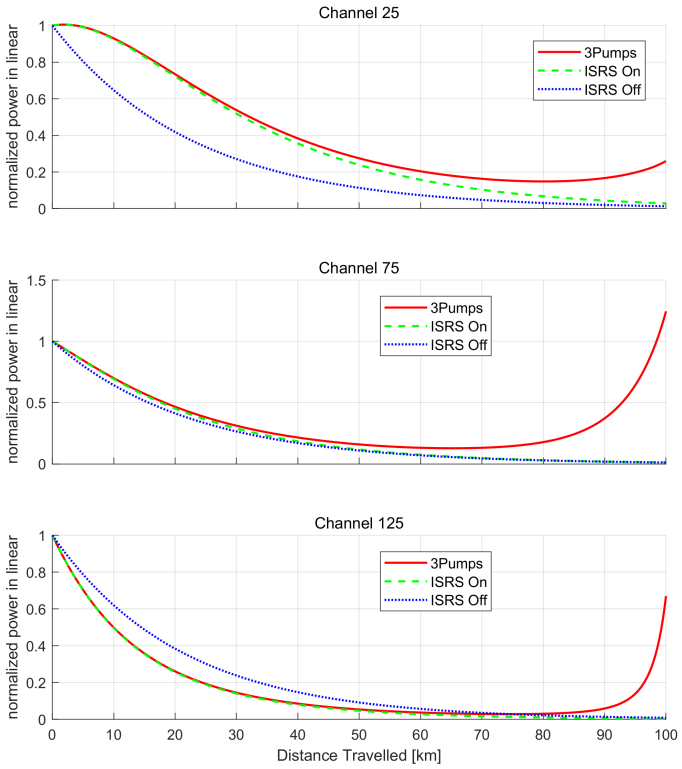

Figure 10: The exact SPPs of three chosen channels ($n_{\text{CUT}} = 25, 75, 125$) under three scenarios, along the 100 km fiber.

$n_{\text{CUT}} + 1$, $m_{\text{ch}} = n_{\text{CUT}}$) and MCI is validated by considering the contribution from the channel on the upper right (i.e., $k_{\text{ch}} = m_{\text{ch}} = n_{\text{CUT}} + 1$). We will substitute the systematic parameters into our analytical solutions to obtain the values for K_{SCI}, K_{XCI}, and K_{MCI}, respectively. These results will then be compared against the numerical integration results (calculated using $N_p = 9$ scheme) obtained by substituting the systematic parameters into Eq. (18), Eq. (19) and Eq. (20).

The following tables summarizes the test results:

Table 2: Comparison of analytical solution and numerical integration K_{SCI}.

n_{CUT}	**SPP case**	K_{SCI} **(Analytical Solution)**	K_{SCI} **(Numerical Integration)**	**Relative Error (Absolute)**
25	C+L+S: ISRS off, no Raman	6.512152199	6.512586241	0.00666%
75		7.878216374	7.878797656	0.00738%
125		9.651628691	9.652790015	0.01203%
25	C+L+S: ISRS on, no Raman	6.530687679	6.538986354	0.12691%
75		7.915737628	7.889977687	0.32649%
125		9.631041558	9.635016564	0.04126%
25	C+L+S: ISRS on + 3 Pumps	6.521553048	6.535498216	0.21338%
75		7.756771908	7.856833564	1.27356%
125		9.225169403	9.411420913	1.97899%

Table 3: Comparison of analytical solution and numerical integration K_{XCI}.

n_{CUT}	**SPP case**	K_{XCI} **(Analytical Solution)**	K_{XCI} **(Numerical Integration)**	**Relative Error (Absolute)**
25	C+L+S: ISRS off, no Raman	0.615268999	0.615160854	0.01758%
75		0.778729619	0.778772677	0.00553%
125		1.004030739	1.004149941	0.01187%
25	C+L+S: ISRS on, no Raman	0.617051916	0.617645998	0.09618%
75		0.782406487	0.779836931	0.32950%
125		1.001597834	1.002217737	0.06185%
25	C+L+S: ISRS on + 3 Pumps	0.616236156	0.617335446	0.17807%
75		0.769787402	0.777276954	0.96356%
125		0.963100106	0.981128237	1.83749%

Table 4: Comparison of analytical solution and numerical integration K_{MCI}.

$\mathbf{n_{CUT}}$	**SPP case**	$\mathbf{K_{MCI}}$ **(Analytical Solution)**	$\mathbf{K_{MCI}}$ **(Numerical Integration)**	**Relative Error (Absolute)**
25	C+L+S: ISRS off, no Raman	1.8940011e-4	1.9134502e-4	1.01644%
75		3.0361974e-4	3.0055126e-4	1.02095%
125		5.0532640e-4	5.0327895e-4	0.40682%
25	C+L+S: ISRS on, no Raman	1.8994654e-4	1.9211567e-4	1.12908%
75		3.0505194e-4	3.0096031e-4	1.35952%
125		5.0410690e-4	5.0231557e-4	0.35661%
25	C+L+S: ISRS on + 3 Pumps	1.8969539e-4	1.9201905e-4	1.21012%
75		3.0013081e-4	2.9997182e-4	0.05300%
125		4.8472634e-4	4.9173957e-4	1.42621%

The validation results confirm the high accuracy of the proposed analytical solutions for the NLI kernels against numerical integration. In the most benign scenario (ISRS off, no Raman), the relative errors for K_{SCI} and K_{XCI} are exceptionally low, typically remaining below 0.02%. Although the errors increase slightly in more complex, Raman-pumped scenarios, the maximum deviation is contained below 2% even in the most challenging cases ($n_{\text{CUT}} = 125$ with ISRS on + 3 Pumps), confirming the model's robustness. We further note that in the context of high dispersion and high symbol rates, the contribution of K_{MCI} becomes significantly small compared to K_{SCI} and K_{XCI}, so it often can be treated as negligible.

Also, the computational efficiency of the proposed analytical solution shows a dramatic improvement compared to numerical integration. Take the baseline scenario ($n_{\text{CUT}} = 25$, C+L+S: ISRS off, no Raman) as an example. The calculation times for the NLI kernels highlight this stark difference:

- K_{SCI}: Analytical solution takes ~ 0.1196 s versus Numerical Integration which takes ~ 73.59 s.
- K_{XCI}: Analytical solution takes ~ 0.1203 s versus Numerical Integration which takes ~ 163.20 s.
- K_{MCI}: Analytical solution takes ~ 0.1155 s versus Numerical Integration which takes ~ 1219.90 s.

The complexity and computational burden of numerical integration increase substantially when moving from K_{SCI} to K_{XCI} and, most significantly, to K_{MCI}, as evidenced by the

corresponding increases in integration time. In sharp contrast, our closed-form analytical solution calculates the values for all three kernels instantaneously and with consistent, low calculation time. This completely eliminates the increased difficulty and time dependency observed in the numerical method, achieving a massive efficiency gain that is essential for rapid system optimization and network planning.

4.3.2 More challenging scenarios

Previous studies often bypassed the complexity of low-dispersion and low-symbol-rate context, enabling them to directly utilize simplified closed-form solutions for K_{XCI} (see Eq. (21)) and avoid a detailed discussion of MCI. However, we will apply the results of our general kernel for $N_p = 7$ to this more complex and challenging environment. This test further highlights the significance of this paper, as it demonstrates that our general analytical solution is not only robust for low-dispersion fibers like NZ-DSF but is also applicable to future extensions. For example, extending the SMF band to the O band would require overcoming a similarly challenging low-dispersion environment.

We extend the verification to a challenging operational regime by extending the SMF to the O band, which is characterized by extremely low (near-zero) dispersion. Specifically, a dispersion of $\approx \mathbf{0.1}$ ps$^{\mathbf{2}}$/km was employed. The system symbol rate is reduced to $\mathbf{10}$GBaud (still utilizing an SRRC filter with a roll-off factor of 0.1), and the channel spacing is set to $\mathbf{12.5}$GHz. This combination of low dispersion and low symbol rate significantly enhances the efficiency of MCI and XCI, thereby creating the most challenging scenario for NLI prediction. The validation test plan will be executed across the three distinct SPP cases described previously: ISRS off/no Raman, ISRS on/no Raman, and ISRS on/+3 Pumps. For these tests, we still examine the performance across the $n_{\text{CUT}} = 25, 75,$ and 125 channels as before.

The test results are presented below:

Table 5: Comparison of analytical solution and numerical integration K_{SCI}.

$\mathbf{n_{CUT}}$	**SPP case**	$\mathbf{K_{SCI}}$ **(Analytical Solution)**	$\mathbf{K_{SCI}}$ **(Numerical Integration)**	**Relative Error (Absolute)**
25	C+L+S: ISRS off, no Raman	1.204662001	1.20474	0.00672%
75		1.204565262	1.204654909	0.00744%
125		1.204074929	1.204219429	0.01200%
25	C+L+S: ISRS on, no Raman	1.208089053	1.209627646	0.12720%
75		1.210300503	1.206364882	0.32624%
125		1.201506583	1.202000294	0.04107%
25	C+L+S: ISRS on + 3 Pumps	1.206398469	1.208982374	0.21373%
75		1.185981813	1.201297252	1.27491%
125		1.150849842	1.174106698	1.98081%

Table 6: Comparison of analytical solution and numerical integration K_{XCI}.

$\mathbf{n_{CUT}}$	**SPP case**	$\mathbf{K_{XCI}}$ **(Analytical Solution)**	$\mathbf{K_{XCI}}$ **(Numerical Integration)**	**Relative Error (Absolute)**
25	C+L+S: ISRS off, no Raman	1.204633966	1.204714503	0.00669%
75		1.204521709	1.204612409	0.00753%
125		1.20402808	1.204174467	0.01216%
25	C+L+S: ISRS on, no Raman	1.208127289	1.209583193	0.12036%
75		1.210210402	1.206259534	0.32753%
125		1.201107219	1.201854501	0.06218%
25	C+L+S: ISRS on + 3 Pumps	1.206530279	1.208975009	0.20222%
75		1.190694093	1.202299881	0.96530%
125		1.154947124	1.176565479	1.83741%

Table 7: Comparison of analytical solution and numerical integration K_{MCI}.

$\mathbf{n_{CUT}}$	**SPP case**	$\mathbf{K_{MCI}}$ **(Analytical Solution)**	$\mathbf{K_{MCI}}$ **(Numerical Integration)**	**Relative Error (Absolute)**
25	C+L+S: ISRS off, no Raman	1.214549419	1.21463619	0.00714%
75		1.214647436	1.214745976	0.00811%
125		1.215027982	1.215187256	0.01311%
25	C+L+S: ISRS on, no Raman	1.207602861	1.209017475	0.11701%
75		1.217764274	1.213477224	0.35329%
125		1.217782883	1.218723667	0.07719%
25	C+L+S: ISRS on + 3 Pumps	1.206533399	1.208428876	0.19658%
75		1.19926876	1.209537213	0.84896%
125		1.170518809	1.191880579	1.79227%

The validation results for the low-dispersion and low symbol rate test scenario further confirm the high accuracy and robustness of our analytical solution. In the two more benign scenarios, ISRS off/no Raman and ISRS on/no Raman, the relative errors for all three kernels (K_{SCI}, K_{XCI}, and K_{MCI}) remain very low, with the maximum error observed being below 0.36%. Even in the most complex scenario (ISRS on + 3 Pumps), the analytical solutions remain highly accurate. The maximum relative error for all kernels is contained below 2%, specifically observed as 1.98081% for K_{SCI}, 1.83741% for K_{XCI}, and 1.79227% for K_{MCI} (all at $n_{\text{CUT}} = 125$).

Under the current low-dispersion conditions, the MCI effect is no longer negligible. A key observation is that for all three chosen n_{CUT} channels, the values of all three interference kernels (K_{SCI}, K_{XCI}, and K_{MCI}) are nearly identical. The reason is that when both the dispersion and the channel bandwidth are very low, all chosen n_{CUT} and their nearest neighboring channels fall within the slow-decay regime. This results in their respective decay characteristics being very similar, which, in turn, explains why the values of K_{SCI}, K_{XCI}, and K_{MCI} are close to each other.

5 Extensions and Applications

Through the tests above, we demonstrate that our closed-form solutions are accurate, computationally efficient, and robustly applicable to all kinds of context in ultra-wide band and long-haul optical fiber transmission system. Building upon the general closed-form solution for the NLI kernel derived in this thesis, future work will first focus on achieving full support for the $N_p = 9$ model. Another crucial future task is optimizing the code structure

and quality to meet the demands of real-time computation. The current implementation already utilizes C/MEX files to link our derived analytical solution with the MATLAB environment, serving as the essential first step toward the ultimate goal of achieving a real-time MEX code deployment. Performance analysis indicates that the primary bottleneck for the current computational speed lies in the implementation of the hypergeometric function, specifically the significant overhead introduced by calling MATLAB's built-in function from the C/MEX file. Therefore, a core optimization strategy is to implement a native, high-efficiency hypergeometric function algorithm within the C/C++ environment, thereby eliminating the performance bottleneck associated with cross-environment calls. This optimization is critical as it will unlock the full potential of the P-CFM framework.

Through the polynomial representation of the channel's spatial power profile, the P-CFM can accurately model complex physical scenarios that were difficult to handle reliably with previous approximations, such as systems involving backward Raman amplification, significant inter-channel stimulated Raman scattering (ISRS), low dispersion, low-loss fibers, and lumped loss conditions. Consequently, by providing a true real-time computational engine for this powerful and versatile model, these optimizations will enable its direct application in the real-time performance monitoring of dynamic optical networks, advanced routing and spectrum allocation algorithms, and the design and planning of next-generation ultra-wideband long-haul systems, thus realizing its maximum practical value.

6 Conclusion

The foundational work of this thesis is a series of mathematical transformations designed to simplify the complex kernel integrals for SCI, XCI, and MCI. Through this process, we successfully decomposed these integrals into a weighted sum of more fundamental, real-valued terms, namely I_{nn} and I_{nm}. This decomposition was the critical first step that enabled the derivation of a general closed-form solution. To this end, we constructed a unified integral paradigm and leveraged optimized symbolic computation strategies, ultimately yielding a complete analytical expression for polynomial power profiles up to the seventh order ($N_p = 7$).

A key strength of this approach is its generality; the derived analytical expressions are applicable to all interference types (SCI, XCI, and MCI) and across all physical scenarios. Crucially, they are robust enough to accurately model the complex physical conditions inherent in modern ultra-wideband long-haul systems, such as those with significant inter-channel stimulated Raman scattering (ISRS) and backward-pumped Raman amplification,

which were difficult to handle reliably with previous methods.

By converting computationally intensive integrals into rapidly evaluable analytical formulas, this research provides the direct means to construct a practical and efficient Polynomial Closed-Form Model (P-CFM). This work therefore provides the crucial mathematical groundwork for high-fidelity, real-time physical-layer modeling, which is essential for the intelligent control and optimization of future dynamic and ultra-wideband long-haul optical transmission systems.

References

[1] A. Mecozzi and R.-J. Essiambre, "Nonlinear Shannon limit in pseudolinear coherent systems," *Journal of Lightwave Technology*, vol. 30, no. 12, pp. 2011–2024, 2012.

[2] R. Dar, M. Feder, A. Mecozzi, and M. Shtaif, "Properties of nonlinear noise in long, dispersion-uncompensated fiber links," *Optics Express*, vol. 21, no. 22, pp. 25685–25699, Nov. 2013.

[3] P. Poggiolini et al., "The GN model of fiber non-linear propagation and its applications," *Journal of Lightwave Technology*, vol. 32, no. 4, pp. 694–721, Feb. 2014.

[4] A. Carena, G. Bosco, V. Curri, Y. Jiang, P. Poggiolini, and F. Forghieri, "EGN model of non-linear fiber propagation," *Optics Express*, vol. 22, no. 13, pp. 16335–16362, Jun. 2014.

[5] P. Serena and A. Bononi, "A time-domain extended Gaussian noise model," *Journal of Lightwave Technology*, vol. 33, no. 7, pp. 1459–1472, Apr. 2015.

[6] H. Buglia et al., "A closed-form expression for the Gaussian noise model in the presence of inter-channel stimulated Raman scattering extended for arbitrary loss and fibre length," *J. Lightw. Technol.*, vol. 41, no. 11, pp. 3577–3586, 2023.

[7] H. Buglia, M. Jarmolovicius, L. Galdino, R. I. Killey, and P. Bayvel, "A closed-form expression for the Gaussian noise model in the presence of Raman amplification," *J. Lightw. Technol.*, vol. 42, no. 2, pp. 636–648, 2024.

[8] P. Poggiolini and M. Ranjbar-Zefreh, "Closed-form expressions of the nonlinear interference for UWB systems," in *Proc. Eur. Conf. Opt. Commun. (ECOC)*, Basel, Switzerland, 2022, paper Tu1D.1.

[9] Y. Jiang, A. Nespola, S. Straullu, A. Tanzi, S. Piciaccia, F. Forghieri, D. Pilori, and P. Poggiolini, "Closed-form EGN model with comprehensive Raman support," in *Proc. Eur. Conf. Opt. Commun. (ECOC)*, Frankfurt, Germany, 2024, paper W1B.1.

[10] M. R. Zefreh, F. Forghieri, S. Piciaccia, and P. Poggiolini, "Accurate closed-form real-time EGN model formula leveraging machine learning over 8500 thoroughly randomized full C-band systems," *Journal of Lightwave Technology*, vol. 38, no. 18, pp. 4987–4999, Sep. 2020.

[11] Y. Jiang *et al.*, "Experimental test of a closed-form EGN model over C+L bands," *Journal of Lightwave Technology*, vol. 43, no. 2, pp. 439–449, Jan. 2025.

[12] P. Poggiolini and Y. Jiang, "Recent advances in real-time models for multiband transmission systems," in *Proc. Optical Fiber Communication Conference (OFC)*, 2025, paper Tu3K.2.

[13] P. Poggiolini, "P-CFMs: polynomial power-profile closed-form models related to the GN-model," *TechRxiv*, 2025, doi: 10.36227/techrxiv.174803120.05191968/v2.

[14] A. Bononi, R. Dar, M. Secondini, P. Serena, and P. Poggiolini, "Fiber nonlinearity and optical system performance," in *Springer Handbook of Optical Networks*, B. Mukherjee, I. Tomkos, M. Tornatore, P. Winzer, and Y. Zhao, Eds. Cham, Switzerland: Springer, 2020, ch. 9.

[15] P. Poggiolini, "The GN model of non-linear propagation in uncompensated coherent optical systems," *J. Lightw. Technol.*, vol. 30, no. 24, pp. 3857–3879, 2012, doi: 10.1109/JLT.2012.2217729.

[16] P. Poggiolini, Y. Jiang, Y. Gao, and F. Forghieri, "Polynomial Closed Form Model for Ultra-Wideband Transmission Systems," *arXiv:2508.21563v1 [eess.SP]*, 29 Aug 2025.